

**Best Available
Copy
for all Pictures**

AD-775 843

DAMAGE PROFILES IN SILICON AND THEIR
IMPACT ON DEVICE RELIABILITY

Guenter H. Schwuttke

International Business Machines Corporation

Prepared for:

Advanced Research Projects Agency

1 January 1974

DISTRIBUTED BY:

NTIS

National Technical Information Service
U. S. DEPARTMENT OF COMMERCE
5285 Port Royal Road, Springfield Va. 22151

AD 775843

DOCUMENT CONTROL DATA - R&D

(Security classification of title, body of abstract and indexing annotation must be entered when the overall report is classified)

1. ORIGINATING ACTIVITY (Corporate author) International Business Machines Corporation System Products Division, East Fishkill Hopewell Junction, N. Y. 12533		2a. REPORT SECURITY CLASSIFICATION Unclassified	
		2b. GROUP	
3. REPORT TITLE DAMAGE PROFILES IN SILICON AND THEIR IMPACT ON DEVICE RELIABILITY			
4. DESCRIPTIVE NOTES (Type of report and inclusive dates) Scientific 6 June 1972 to 30 December 1973			
5. AUTHOR(S) (First name, middle initial, last name) Guenter H. Schwuttke			
6. REPORT DATE 1 January 1974		7a. TOTAL NO. OF PAGES 67	7b. NO. OF REFS 20
8a. CONTRACT OR GRANT NO. DAHC 15-72-C-0274		9a. ORIGINATOR'S REPORT NUMBER(S) TR 22.1741	
b. PROJECT, TASK, WORK UNIT NOS.			
c. DOD ELEMENT			
d. DOD SUBELEMENT		9b. OTHER REPORT NO(S) (Any other numbers that may be assigned this report)	
10. DISTRIBUTION STATEMENT			
11. SUPPLEMENTARY NOTES		12. SPONSORING MILITARY ACTIVITY Advanced Research Projects Agency	
13. ABSTRACT This contract work examines the behavior of crystal defects in silicon and their impact on semiconductor device reliability. In Technical Report No. 1 we have shown that crystal defects in the Si surface of MOS capacitors influence MOS capacitance relaxation. It was shown that the time behavior of the deep depletion capacitance relaxation is strongly influenced by residual mechanical saw damage which is sometimes present in standard silicon surfaces after polishing. Using transmission electron microscopy the residual saw damage was identified as microsplittings of the silicon lattice. Microsplittings were shown to vary considerably in density and size across a wafer surface and large differences in microsplit density were found for different wafers. In Technical Report No. 2 evidence was presented that residual mechanical saw damage in wafer surfaces varies with different slicing and polishing procedures. It was also shown that the amount of saw damage is larger in wafers cut from the tail-end relative to wafers cut from the seed-part of the crystal. It is the purpose of this report to substantiate the previously reported findings on saw damage in silicon wafer surfaces and their dependency on the slicing technique. The measurements reported here concentrate on "measurements of damage depth" in as-sliced silicon wafers, on saw damage measurements in wafers sliced horizontally (H-wafers) compared to wafers sliced vertically (V-wafers), and, finally, on the measurement of fracture strength of silicon crystals and on the seed to tail variation of fracture strength in such crystals.			

DAMAGE PROFILES IN SILICON AND THEIR
IMPACT ON DEVICE RELIABILITY

Prepared by: G. H. Schwuttke
International Business Machines Corporation
East Fishkill Laboratories
Hopewell Junction, New York 12533

TECHNICAL REPORT NO. 3

January 1, 1974
Contract Monitor: Dr. C. M. Stickley

Sponsored by:

Advanced Research Projects Agency
ARPA Order No. 2196, Program Code No. P2D10

Form approved budget bureau No.: 22-RD-293



LIST OF INVESTIGATORS

The project is supervised by Dr. G. H. Schwuttke, principal investigator. The following people contributed to the work in the report:

Dr. K. H. Yang, Investigator

Mr. R. G. Dessauer, Investigator

Mr. J. F. Francis, Technical Support

Mr. H. L. Stellefson, Technical Support

CONTENTS

List of Investigators	ii
Table of Contents	iii
Summary	v

Chapter 1

Damage Profiles in Silicon Wafers

After ID Slicing

1.	Introduction	1
2.	Depth of Saw Damage Measurements	4
	2.1 Review of Mechanically Induced Damage in Silicon After Slicing	5
	2.2 Surface Damage Models	11
3.	Problems of Mechanical Damage Studies	12
4.	Damage Measurements	14
	4.1 Experimental Approach	16
	4.2 Measurements of Damage	19
	4.3 Damage Profiles	34
5.	Application of Saw Damage Measurements to H- and V-Silicon Wafers	36
6.	Discussion	38
7.	Summary and Conclusions	41
8.	References	43

Chapter 2

Fracture Strength of Doped Single

Crystal Silicon

1.	Introduction	44
2.	Experimental Approach	44

CONTENTS

3.	Technique Development	45
4.	Measurements of Fracture Strength on Seed and Tail Sections of Silicon Crystals	51
5.	Conclusions	59
6.	References	60

This contract work examines the behavior of crystal defects in silicon and their impact on semiconductor device reliability. In Technical Report No. 1 we have shown that crystal defects in the Si surface of MOS capacitors influence MOS capacitance relaxation. It was shown that the time behavior of the deep depletion capacitance relaxation is strongly influenced by residual mechanical saw damage which is sometimes present in standard silicon surfaces after polishing. Using transmission electron microscopy the residual saw damage was identified as microsplits of the silicon lattice. Microsplits were shown to vary considerably in density and size across a wafer surface and large differences in microsplit density were found for different wafers. In Technical Report No. 2 evidence was presented that residual mechanical saw damage in wafer surfaces varies with different slicing and polishing procedures. It was also shown that the amount of saw damage is larger in wafers cut from the tail-end relative to wafers cut from the seed-part of the crystal.

It is the purpose of this report to substantiate the previously reported findings on saw damage in silicon wafer surfaces and their dependency on the slicing technique. The measurements reported here concentrate on "measurements of damage depth" in as-sliced silicon wafers, on saw damage measurements in wafers sliced horizontally (H-wafers) compared to wafers sliced vertically (V-Wafers), and, finally, on the measurement of fracture strength of silicon crystals and on the seed to tail variation of fracture strength in such crystals.

DAMAGE PROFILES IN SILICON WAFERS AFTER ID SLICING

1. INTRODUCTION

Large-volume oriented manufacturing slicing of silicon crystals into thin wafers is economical only if inside diameter (ID) diamond saws are used. Consequently, ID slicing is the favored technique used in semiconductor manufacturing. For ID slicing silicon crystals can be mounted horizontally and thus are cut by a blade in the vertical position or the crystal is mounted vertically and is thus cut by a blade in the horizontal position. The two modes of crystal cutting practiced in manufacturing slicing are shown schematically in Figs. 1a,b.

Previously, it was found that the amount of residual saw damage still present in the silicon surface after chemical-mechanical polishing seems to depend on the wafer position in the crystal, and also seems to vary considerably with the slicing technique. Higher MOS capacitor/wafer yield was obtained on wafers cut close to the seed part of the crystal and also better yield was obtained on H-wafers (horizontally sliced, Fig. 1a) as compared to V-wafers (vertically sliced, Fig. 1b).^{1,2} Such results were taken as an indication that the seed part of a crystal is less susceptible to saw damage than the tail part and that the horizontal slicing mode is more gentle than the vertical one.

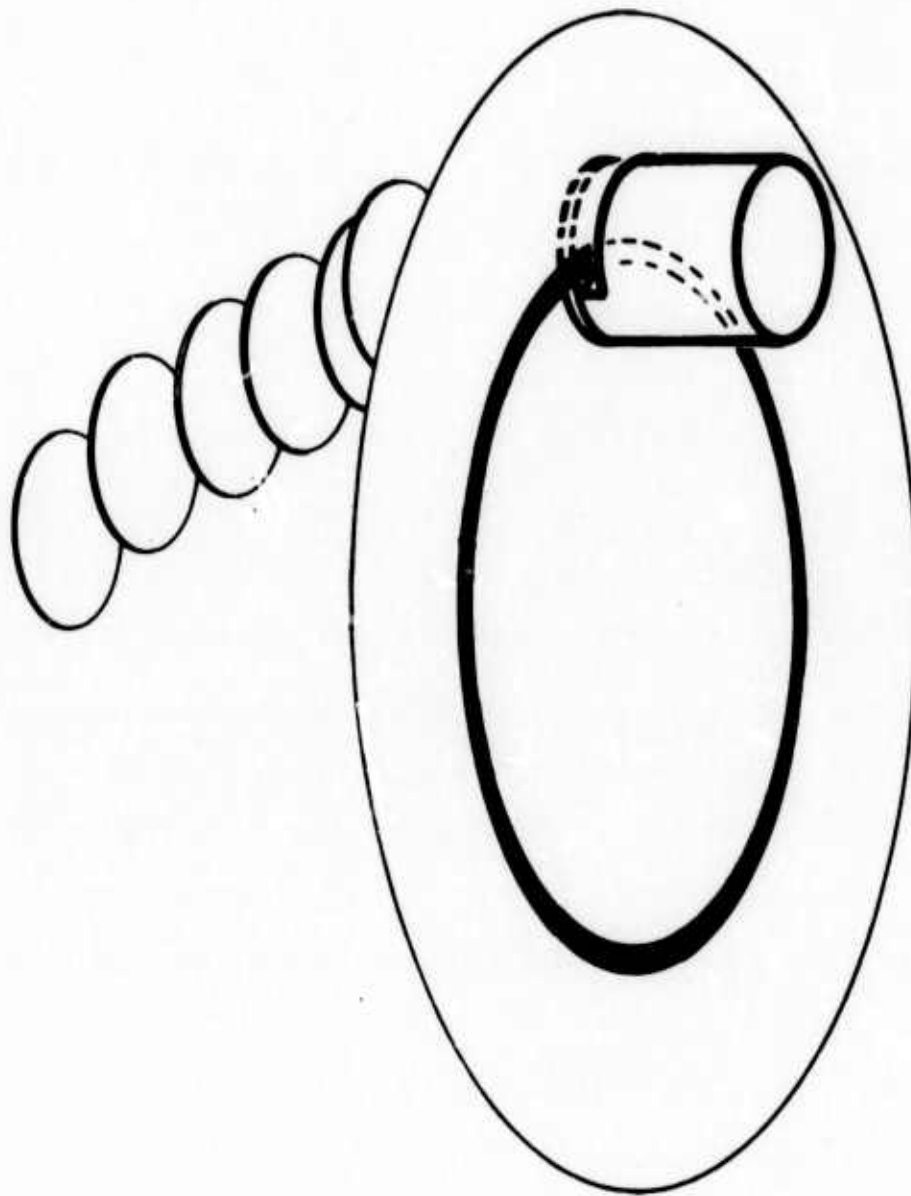


Fig. 1a. Horizontal ID slicing of crystal (H-wafer).

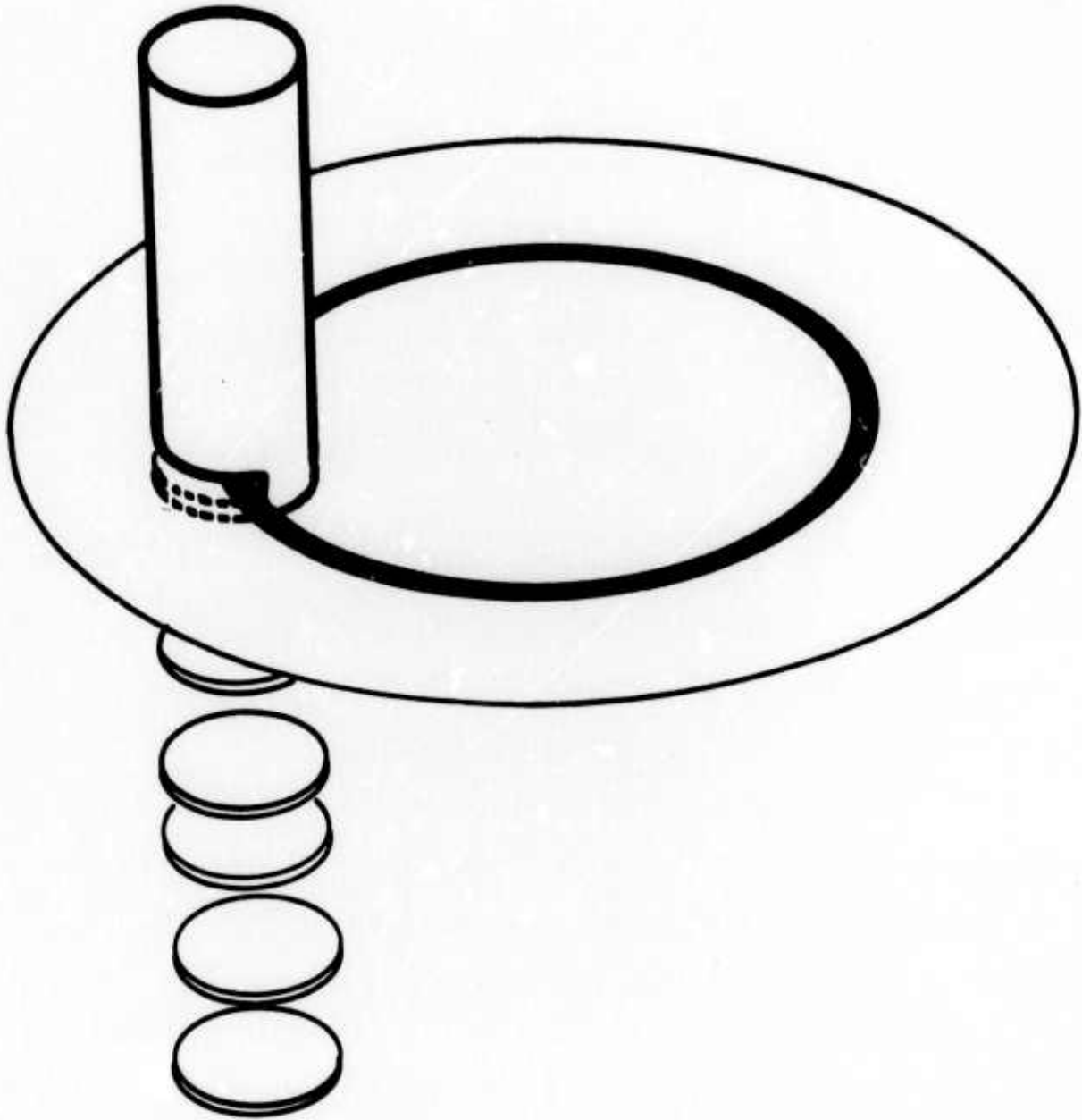


Fig. 1b. Vertical ID slicing of crystal (V-wafer).

In the following this contention is further confirmed through measurements of "damage depth" and "damage profiles" in silicon wafers sliced under manufacturing conditions.

2. DEPTH OF SAW DAMAGE MEASUREMENTS

The intent of damage measurements in silicon wafers is to associate a characteristic depth of damage with a particular wafer shaping operation, such as sawing, lapping, and polishing. If this value is known, the damaged layer can be chemically removed with a minimum of material wasted. Complete removal of mechanical damage in wafer surfaces has become more important for advanced silicon device technologies than ever before.^{1,2}

Previous investigations were applied to measure damage as a result of slicing, lapping, and polishing.³⁻⁶ The agreement between the differently measured values of saw damage is quite poor indicating certain difficulties with standard measurement techniques. To clarify such disparities on depth of damage values as reported in the literature and also to demonstrate the need for a different approach to measure "depth of damage", this chapter first reviews present concepts of "saw damage depth", subsequently formulates problems encountered in

mechanical damage studies, then discusses techniques precise enough to evaluate "depth of damage" in wafers cut from different positions in the crystal, and finally applies this technique to H- and V-sliced wafers.

2.1 Review of Mechanically Induced Damage in Silicon Crystal After Slicing

The concept of "depth of damage" has not been applied consistently in the literature. Some investigators assign this term to the maximum extent of the worked layer that can be measured directly. In comparison, others refer to "depth of damage" as the depth detectable by electrical phenomena, and here the depth of damage is deduced indirectly from the electrical measurements.

Principal direct methods used to evaluate damage are: the taper section metallographic method,⁴ transmission electron microscopy,⁶ and the etch rate method.³ The principal indirect methods are the photomagneto electric (PME) effect⁷ and the photoconductive decay (PCD) method⁷ and recently the MOS capacitance relaxation technique.^{1,2} The electrical techniques⁷ were used in germanium, while the MOS capacitance technique was very successful in characterizing silicon after chem-mech polishing.^{1,2}

The different techniques are briefly reviewed in the following:

Taper Section Method

The taper section method involves sectioning the abraded surface at a nominal angle of $\sim 5^\circ$, which produces a geometrical magnification of 10:1 perpendicular to the section line. Optical magnification of the selectively etched surface⁴ reveals the damage depth directly. The depth of damage is taken from the prominent crest of the surface irregularities to the extremities of the perturbed layer.

Transmission Electron Microscopy

The silicon sample is abraded on one side; the undamaged side is chemically thinned to $\sim 2\mu\text{m}$. A tilting stage is employed to determine the exact nature of the damage, i.e., dislocation or cracks. The depth-of-damage values are obtained by progressively removing the abraded surface with CP4 ($5\text{HNO}_3:3\text{HF}:3\text{CH}_3\text{OOH}$) etch to reveal the structure. The resultant surface is examined with an optical microscope, and the damage depth is determined by changing the focus ($\pm 1\mu\text{m}$ estimated accuracy).

Etch Rate Method

The dependence of etch rate on crystal perfection is used to determine an average damage depth. This method depends on the fact that damaged material etches more rapidly than undamaged material. The abraded samples are weighed and then etched to remove a thin surface layer; the etch rate is computed from the weight loss per unit etch time. This procedure is continued until the etch rate becomes constant. The depth at which this constancy occurs is termed the depth of damage.

Electrical Measurements

The photomagneto electric (PME) effect and the photoconductive decay lifetime (PCD) method are used to detect variations in the recombination rate of excess minority carriers below the surface. The surface recombination rate is enhanced at the damaged surface because of the high density of recombination centers associated with the worked layer. As the surface layer is removed through etching, the carrier recombination rate decreases and approaches a steady-state condition. The weight loss method is used to determine the depth at which the rate of carrier generation and recombination reaches equilibrium. Recently, electrical measurements based on storage time measurements

of MOS capacitors pulsed into deep depletion have successfully been used to characterize residual saw damage in chemical-mechanical polished silicon wafer surfaces. For details on this technique see Technical Report No. 2 of this contract.

In Table I, we have compiled information showing the expected precision and sensitivity of the various techniques used to measure the damaged layer. However, one must be aware that the precision of the methods listed in Table I is subject to controversy.^{4,8} Table II gives various reported values for saw damage in silicon. These results were obtained with different methods and compare the depth of damage for the OD and ID sawing techniques. The OD saw utilizes the outer diameter of the blade for cutting, whereas in the ID method the inner diameter of the blade is used. The large differences in the results shown in Table II suggest either that the experimental methods are inconsistent or that the sawing operation produces a distribution of damage depths rather than a single value. It is also likely that both of these conditions are operative and produce this variation in data. An exact comparison between these techniques used to determine damage depth is complicated by the fact that some are sensitive to the maximum depth of damage⁴ and others yield an average value.³ Some of these difficulties have been resolved in a comparative study of polishing damage reported by Stickler and Faust.⁵

TABLE I - Sensitivity of Various
Measuring Techniques

Method	Advantages	Disadvantages	Reference
Etch Rate	1. Experimentally simple and reliable.	1. Etch rate may be exaggerated by temperature increase due to heat of reaction. 2. The change in surface area can introduce a 2-5% error in the depth of damage measurement. 3. The nature of the damage cannot be determined with this method.	7 3
Taper Section	1. Experimentally simple. 2. Yield direct evidence of damage structure and the maximum extent of the worked layer.	1. The depth of damage may be greater because of aggravation of the damaged layer during preparation of the taper section.	3
Transmission Electron Microscopy	1. The detailed nature of the damage can be determined.	1. The technique cannot be employed to evaluate damage depths greater than the penetration depth of electrons in the material, 2000Å.	6
PME	1. Sensitive to the electrical properties of the material.	1. Experimentally complex. 2. Measurements are difficult on silicon because of its tendency to have very high recombination velocity values even on thoroughly etched surfaces unless special chemical treatments are used.	
MOS	1. Simple, very sensitive to residual surface damage after polishing.	1. Excellent for mapping silicon wafers.	1,2

TABLE II - Typical Values of Saw Damage in Silicon

Investigators	Exp. Method	Depth of Damage [Microns]	Sawing Technique
R. Stickler and G. R. Booker	Planar Polishing (Polish-Etch)	43-47	OD Saw
J. Faust	Constancy of Etch-Rate	10-18	OD, Feed Rate 1/2 in/min, 3600 rpm Blade Rotation
J. Faust	Constancy of Etch-Rate	~3.5	ID Saw
F. J. Saccocio and W. McKeown	SOT Topography	≤12.5	ID HAMCO Saw 3000 rpm Blade Rotation

2.2 Surface Damage Models

Present models of surface damage respond either to the type of structural defects or to the effects of these crystal flaws on the electrical properties of the material.

The structural model relates the abrasion process to gouging particulate matter from the crystal surface by a cleavage and/or fracture mechanism. Wolff demonstrated the existence of cleavage in abraded material through optical goniometry.⁹ The orientation dependence of damage, as shown by Faust,³ also substantiates the conclusion above. According to this author³ and others¹⁰ three irregular damage zones are created at different depths in the crystal when the surface is abraded. The surface layer consists of microcracks, dislocation networks, and elastically strained regions. The interior zone contains dislocation networks and/or single dislocations and microsplits.^{1,2} The density of dislocation and/or microsplits decreases with increasing depth into the crystal until finally only unperturbed material exists. This structure was first suggested by Faust¹⁰ and later confirmed by Stickler and Booker using transmission electron microscopy.⁶ The microsplit model was recently confirmed through work reported under this contract.^{1,2}

The electrical model of surface damage, as formulated from Buck's experiments with PME and PCD, requires a thin layer of very low lifetime material at the surface. The recombination centers in the distorted layers are assumed to be dislocations and vacancies. The acceptor action of these defects in Si is well known.

The electrical model of surface damage was recently refined using the MOS storage time recovery from deep depletion to its equilibrium value.^{1,2} This value is proportional to generation lifetime and a sensitive indicator of crystal perfection.

A damage model based on these ideas is shown schematically in Fig. 2.

3. PROBLEMS OF MECHANICAL DAMAGE STUDIES

Numerous investigators have contributed to the present understanding of depths of damage^{3,7} and to the nature of mechanical damage in silicon.^{6,7,10} However, these measurements were made under rather idealized conditions and through methods not readily adaptable to a cause-and-effect evaluation of the actual wafer shaping process in semiconductor manufacturing. Damage problems accompanying the shaping processes in semiconductor manufacturing can be formulated as follows: (a) determine the depth of damage after various wafer shaping operations, (b) define the true nature of the crystal defects, and (c) optimize the crystal shaping methods.

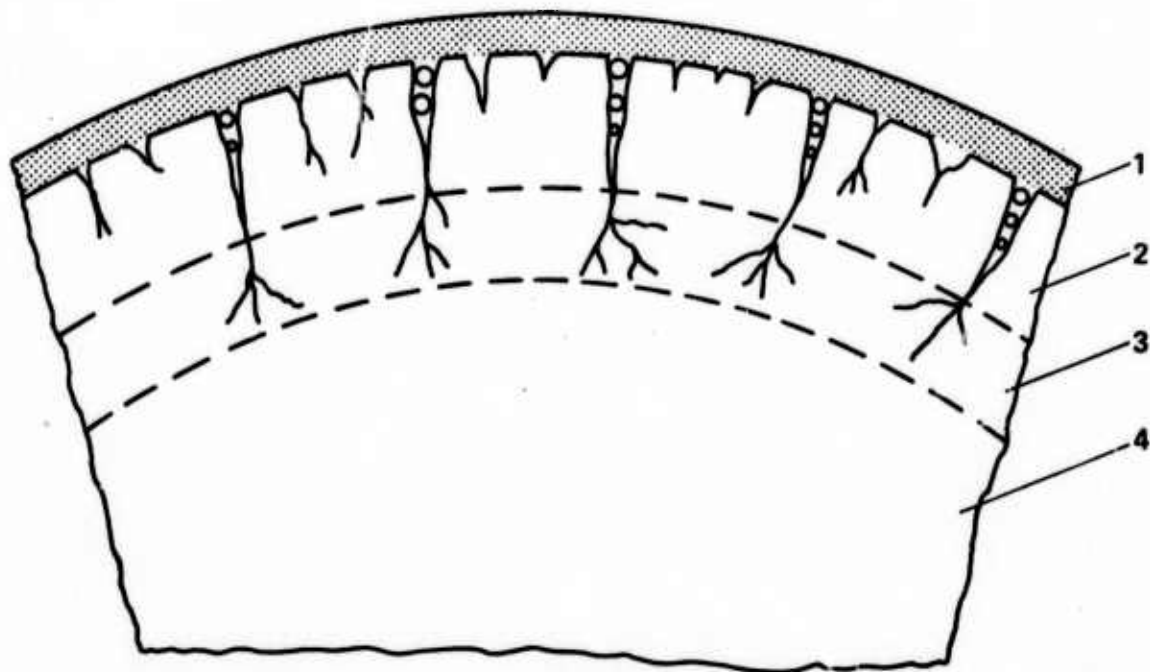


Fig. 2. Damage model showing simplified outline of structure of sawed single crystal surface.

1. Cracks and dislocation network.
2. Dislocation and cracks.
3. Microsplits.
4. Perfect crystal.

The investigations reported in the following section of this paper are primarily directed toward the problems listed under (a) and consequently can be applied to (c).

4. DAMAGE MEASUREMENTS

The first part of this work is based on data obtained previously and contributes greatly to the understanding of saw damage in the context of the present work.¹¹ Dislocation-free silicon crystals of 1.5 inch diameter were chosen for this investigation. The (111) crystals were grown boron-doped of varying resistivity. The crystals were prepared for sawing by fixing the crystals onto a wax-covered (Duali Tan wax) ceramic block. The lower ends of the crystals were uniformly covered with wax after vertical mounting. A commercial HAMCO ID saw was used, with a 200-grit blade, 10 mils thick. The saw blade rotation was maintained at 3600 rpm with an observed cutting rate of 1-1/4 in/min. The saw was operated in a production environment, and no special cutting procedures were employed in the experiments.

Figure 3 depicts the schematic of a wafer identification system used. The location of the wafer face relative to the saw blade is identified by arbitrarily labeling the wafer surface which is attached to the crystal bulk during cutting as A. The wafer surface on the opposite side of the blade is designated B. Samples are selected from the front, middle, and end of the crystal, and their surfaces are identified accordingly as A or B samples.

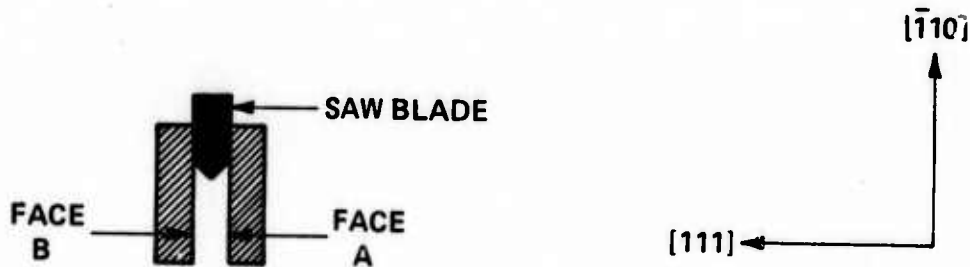
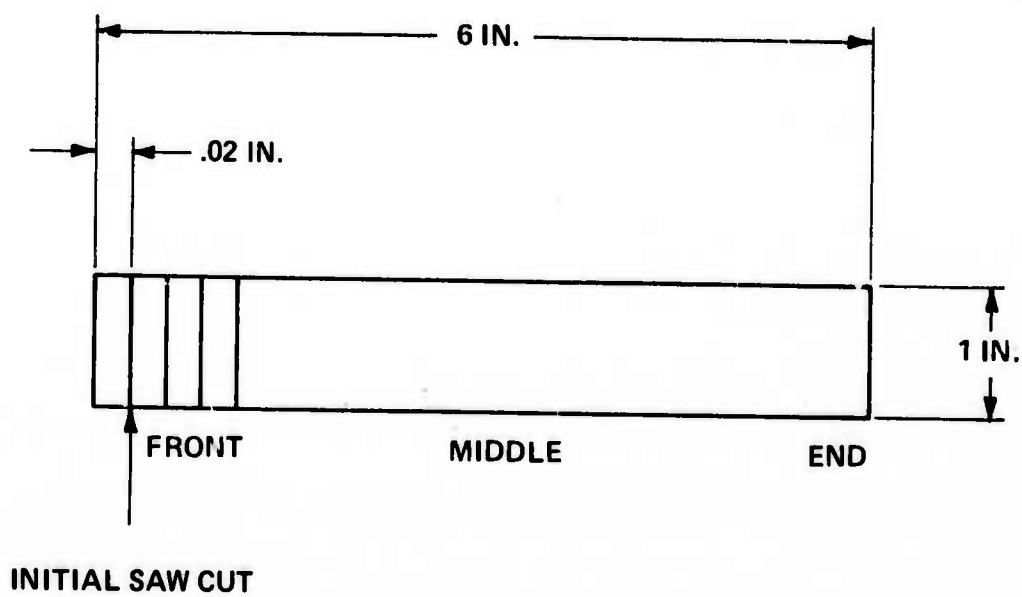


Fig. 3. System of identification used in this report.

4.1 Experimental Approach

SOT topography records topographs of entire crystal wafers several inches in diameter even in the presence of elastic strains.¹² Saccocio and McKeown¹³ have shown that a single SOT topograph of a step-etched wafer can reveal the extent and also the distribution of damage in a saw-cut silicon slice. We have applied this technique to characterize crystal shaping processes in terms of saw damage. Our approach is shown schematically in Fig. 4. Accordingly, the sawed wafer contains a damage zone on both the A and B surfaces (not necessarily equal in depth). For the analysis of contiguous A and B surfaces, two adjacent wafers are used. The A surface on one wafer and the B surface of the other slice are step-etched in a solution of 3 parts $\text{HC}_2\text{H}_3\text{O}_2$, 2 parts HNO_3 and 1 part HF. Thus a series of steps or mesas is made through the damaged layer. Each step exposes a different level of damage. These steps are shown schematically in Fig. 4 and are labeled from 0 to 4. The step height is measured as described by Saccocio and McKeown,¹³ which is satisfactory for evaluating gross damage. Samples can be examined incrementally to a greater depth in the same way simply by masking one half of the wafer on a line normal to the first set of steps and subsequently step-etching the material from the exposed half. In this manner samples were evaluated in increments of $\sim 2.5\mu\text{m}$ down to a depth of $\sim 40\mu\text{m}$ or more.

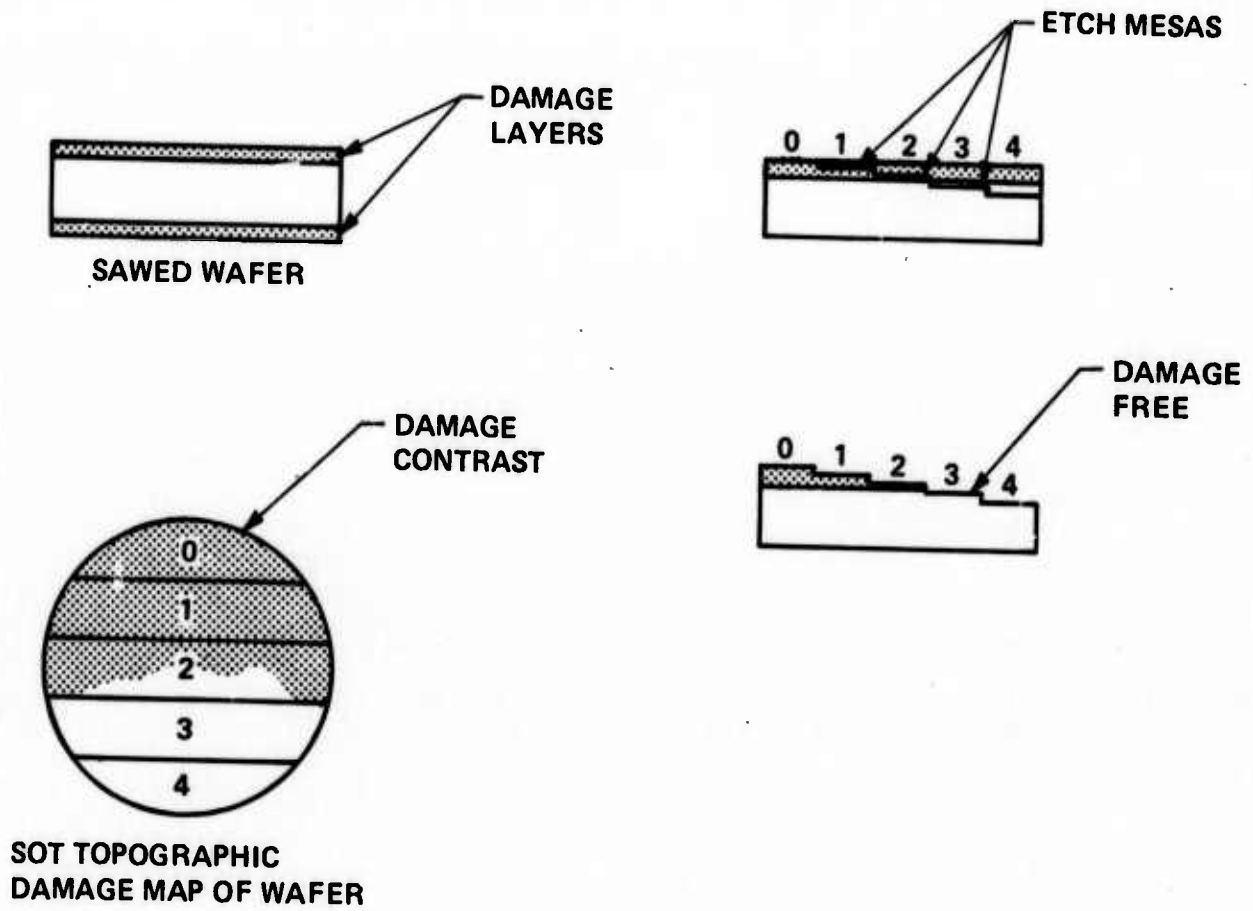


Fig. 4. SOT topography and damage distribution in wafer.

A typical SOT topograph of a sawed wafer after step-etching is shown in Fig. 5a. It is seen that the damage contrast clearly delineates the boundaries between damaged and undamaged material. The individual saw damage per wafer is displayed in a more quantitative way through damage maps constructed as shown in Fig. 5b. Such maps are obtained by measuring the step height of the mesas and relating this information to a schematic of the damage contrast as obtained from the SOT topograph.

The damage contrast at known increments below the surface represents a direct measure of the extent and distribution of saw damage. The step height measurements are accomplished either through light section microscopy or light interferometry. In most cases both measurements agreed well within experimental error. However, in some cases the step height measurements were in doubt because of the irregular surface produced by sawing. For these samples height measurements were obtained by evaporating a 2000\AA silver film over the irregular surface, which improved surface planarity of almost all wafers. The average step height measurement after film evaporation was usually within 30% of the average value obtained directly from the irregular surface.

4.2 Measurements of Damage Depth

Reproduced from
best available copy.

Front Cuts

Figure 5a is a SOT topograph of saw damage in the B surface of a wafer cut from the front of the crystal. The intensity of the x-ray diffraction contrast indicates the degree of deformation in the crystal. The dark contrast layer in Fig. 5a at position 0 represents the crystal damage immediately after cutting. The reduction of contrast after the first step (1) is appreciable and extends uniformly across the wafer. It is interesting to note that after the second step (2) and after each following step, the damage contrast is nonuniformly distributed across the wafer. The areas of the topograph that show uniform or nonuniform contrast are designated I and II, respectively. The damage map obtained from this topograph is shown in Fig. 5b. The saw direction is also indicated in this figure. The damage map illustrates two separate sources of damage: (I) a uniform mode, which reflects blade wear, grit size, rpm, etc.; and (II) a nonuniform mode of damage, which is related to the direction of the saw cut.

If the two damage types are assumed to be independent, the damage map of Fig. 5b indicates a nonuniform depth of damage (in the direction of saw cut) of $\sim 20\mu\text{m}$.

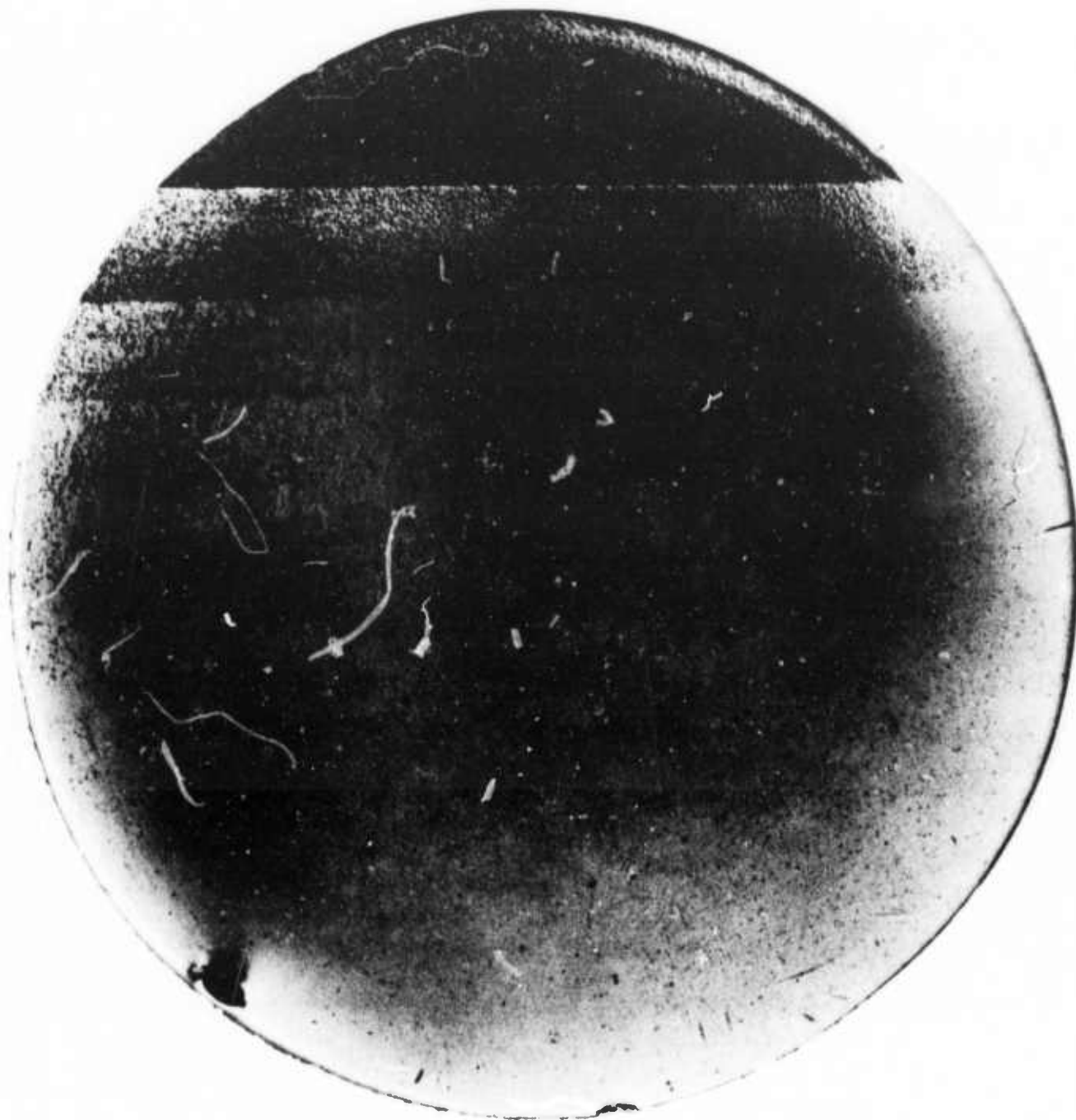
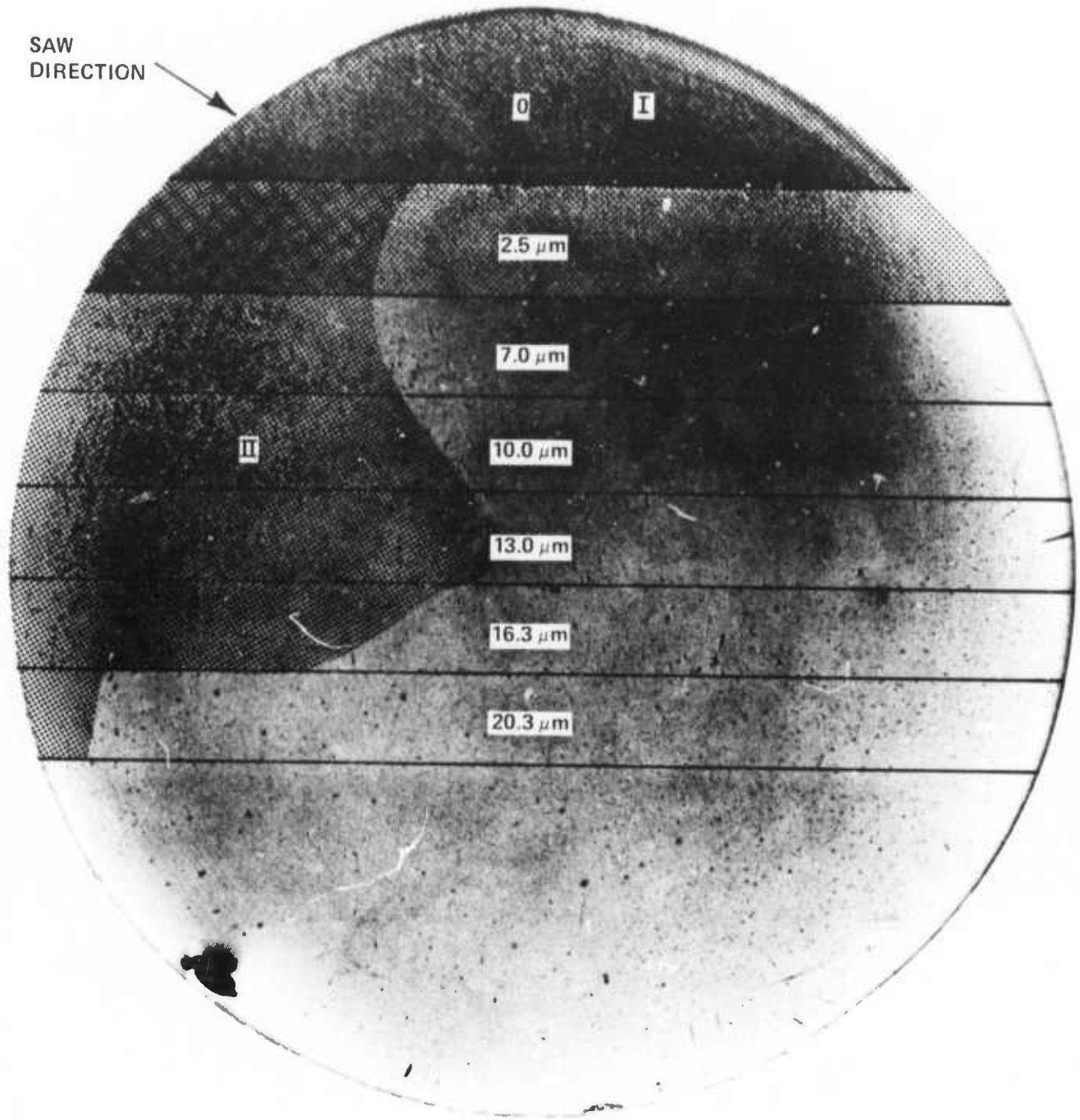


Fig. 5a. SOT topograph of saw damage in B surface of wafer cut from the front of crystal. Note reduction of x-ray contrast after initial etch step. Homogeneous and inhomogeneous damage zones are labeled I and II respectively.

DAMAGE MAP: FRONT B



DAMAGE DEPTH:  UNIFORM ~ 2.5 μm
 NONUNIFORM ~ 20.3 μm
 OVERLAP

Fig. 5b. Damage map corresponding to Fig. 5a.

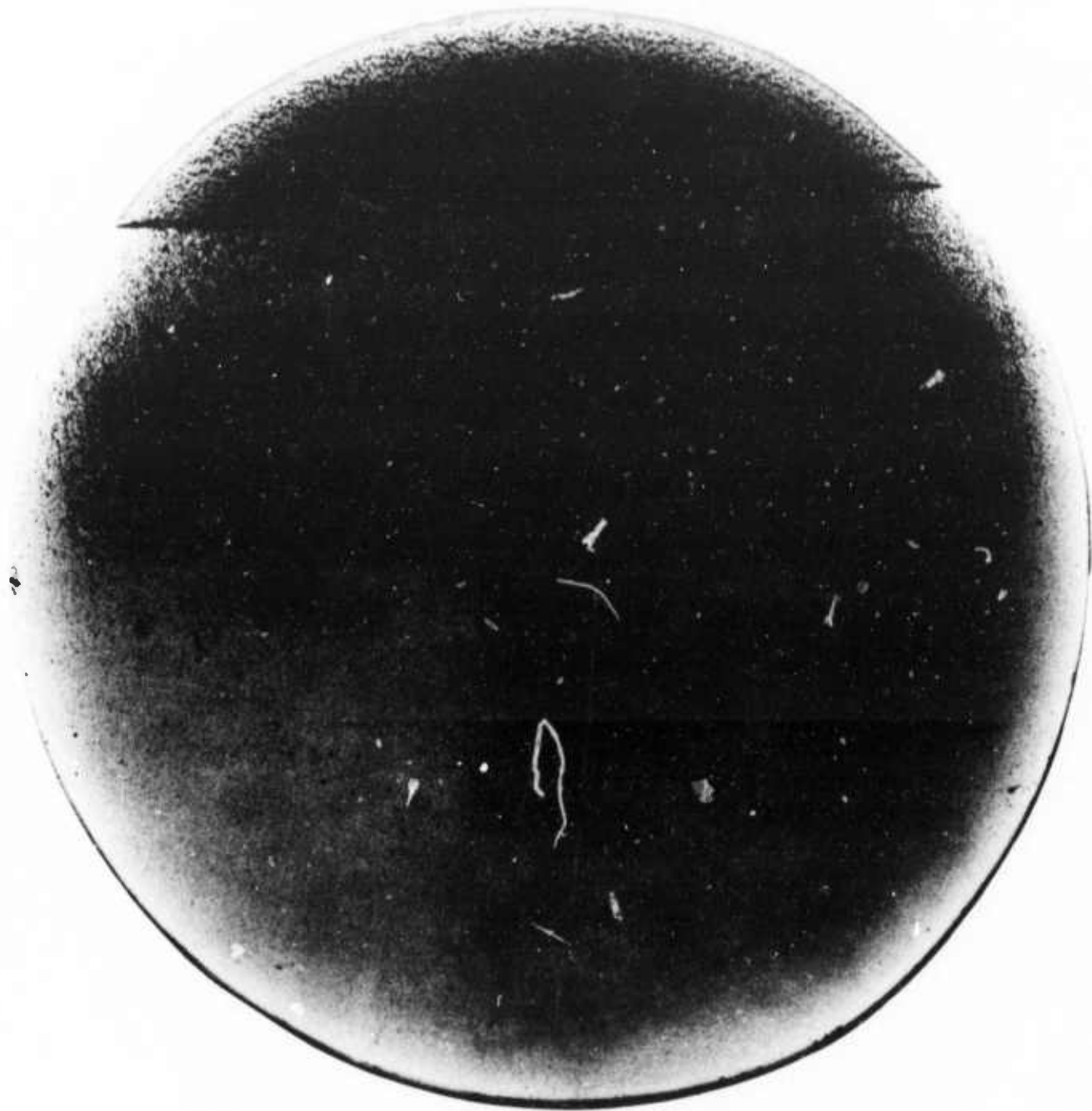
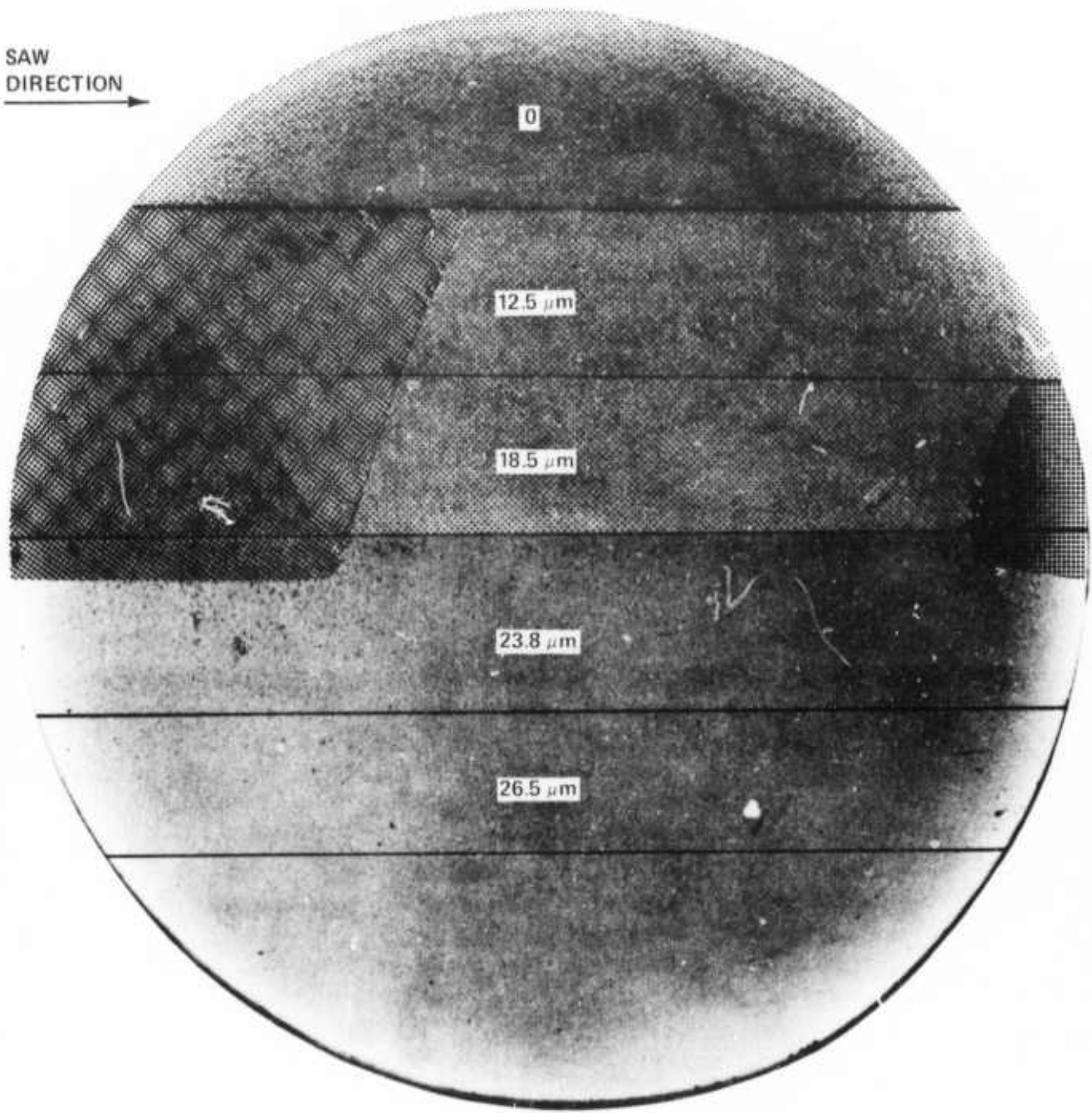


Fig. 6a. SOT topograph of damage in surfaces of front wafer.

Reproduced from
best available copy.

DAMAGE MAP: FRONT A

SAW
DIRECTION
→



DAMAGE DEPTH:  UNIFORM ~ 18.5 μm
 NONUNIFORM ~ 23.8 μm
 OVERLAP

Fig. 6b. Damage map corresponding to Fig. 6a.

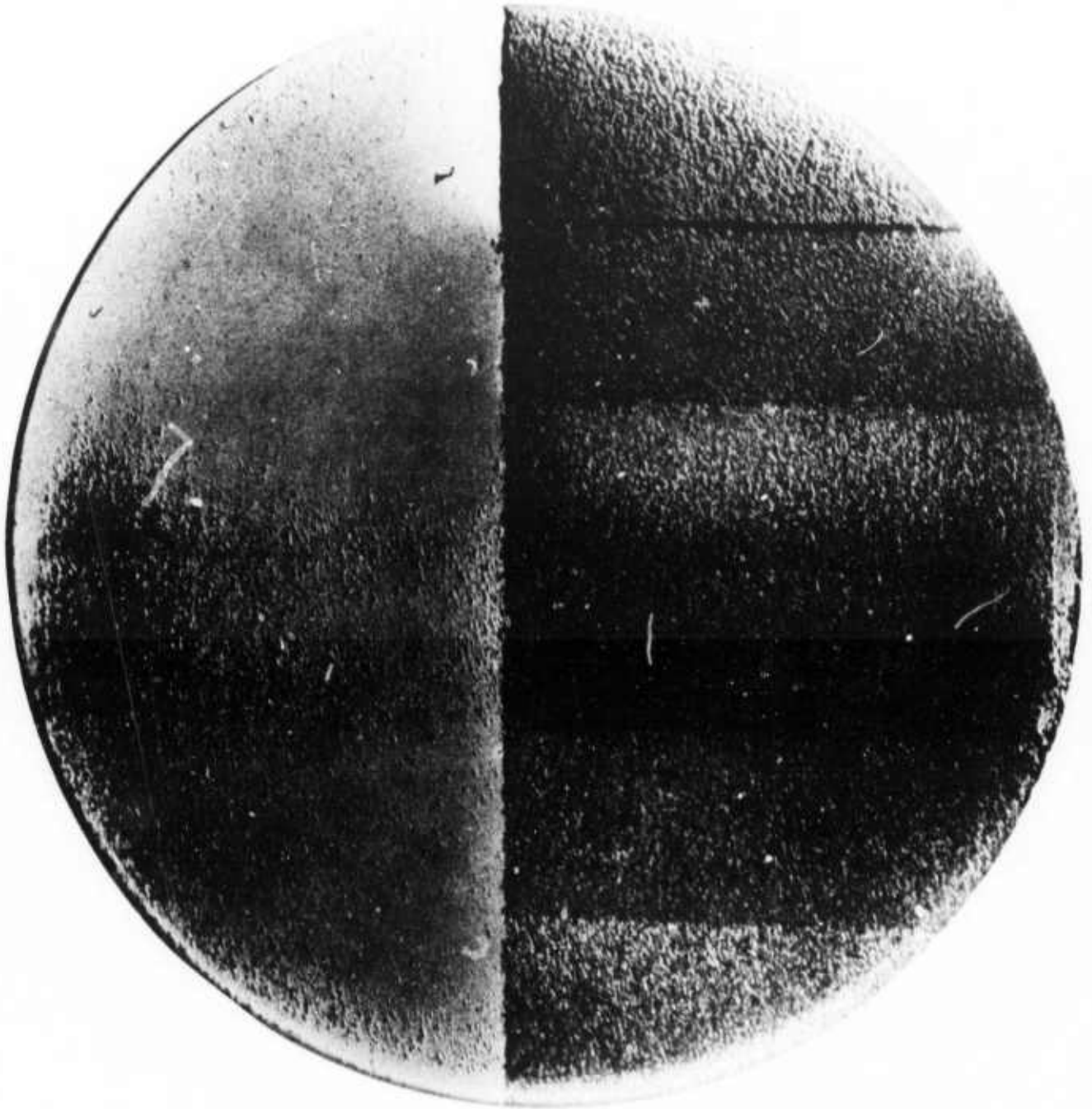
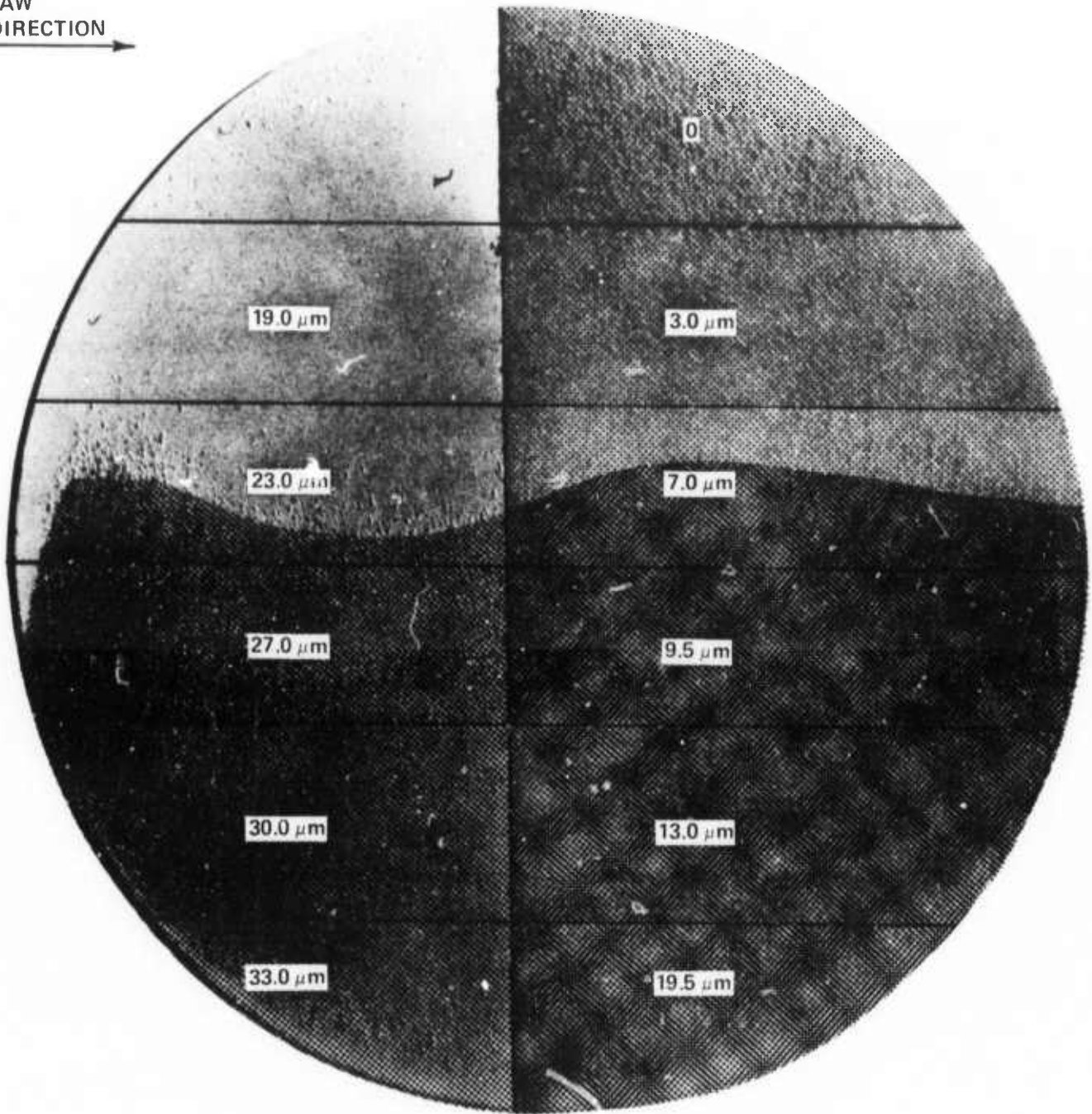


Fig. 7a. SOT topograph of damage in A wafer, middle cut.

DAMAGE MAP: MIDDLE A

SAW
DIRECTION
→



DAMAGE DEPTH:  UNIFORM ~ 13.0 μm
 NONUNIFORM > 33.0 μm
 OVERLAP

Fig. 7b. Damage map corresponding to Fig. 7a.

A SOT topograph of the corresponding A surface is shown in Fig. 6a, and a damage map of the same topograph is shown in Fig. 6b. (Note that the surfaces in Figs. 5a and 6a were separated by the same cut.) As shown previously, the maximum contrast occurs in the unetched mesa. In Fig. 6a the damage contrast is reduced uniformly after each step until its final elimination $\sim 24\mu\text{m}$. It should be noted that the incremental variations in x-ray contrast as seen in the topographs of Figs. 5a and 6a give a good qualitative picture of the damage distribution in the crystal interior.

Middle Cuts

A SOT topograph of the A surface of a sample selected from the middle of the crystal is seen in Fig. 7a. Note that this time the damage is more extensive and nonhomogeneous across the A surface than across the B surface. (Note that the A surface of the front cut did not contain nonuniform damage.) The damage map* of Fig. 7b shows that the uniform damaged ends $13\mu\text{m}$ below the surface, whereas the nonuniform component extends

*The damage map is constructed such that the mesa opposite the original surface is at nearly the same depth as the final step of the first etching ($-19.5\mu\text{m}$). This is accomplished by measuring the total step heights of the first set of steps ($-19.5\mu\text{m}$) and then thinning chemically one half of the wafer to the same depth. This depth can be measured relative to the original surface (adjacent mesa) and the remaining step heights are measured relative to this value.

deeper than $33\mu\text{m}$. The corresponding B surface shows homogeneous damage plus strong contrast striations (Fig. 8a). In addition, the twice-etched half of the wafer displays peripheral damage. The depth of damage, as displayed in the map (Fig. 8b), is $12.5\mu\text{m}$ for the striations and $27\mu\text{m}$ for the edge damage. Note that the underlying uniform damage disappears at about the same depth as the striations and that the individual striae end at nearly the same depth.

End Cuts

The x-ray topographic images of the A and B surfaces of wafers cut from the end of the crystal are essentially identical to Figs. 7a and 8a and are shown in Figs. 9a and 10a. The nonuniform damage in the A surface (Figs. 9a) has a polished appearance similar to the one shown in Fig. 7a; the nonuniform damage in the B surface (Fig. 10a) consists of striations and edge damage of the type shown in Fig. 8a. The damage map of the A surface is shown in Fig. 9b. The uniform damage is removed after $8.5\mu\text{m}$, and the nonuniform damage is more than $32.5\mu\text{m}$ deep. The B surface map (Fig. 10b) indicates $\sim 9.5\mu\text{m}$ of uniform damage and $35.5\mu\text{m}$ of nonuniform edge damage.

Reproduced from
best available copy.

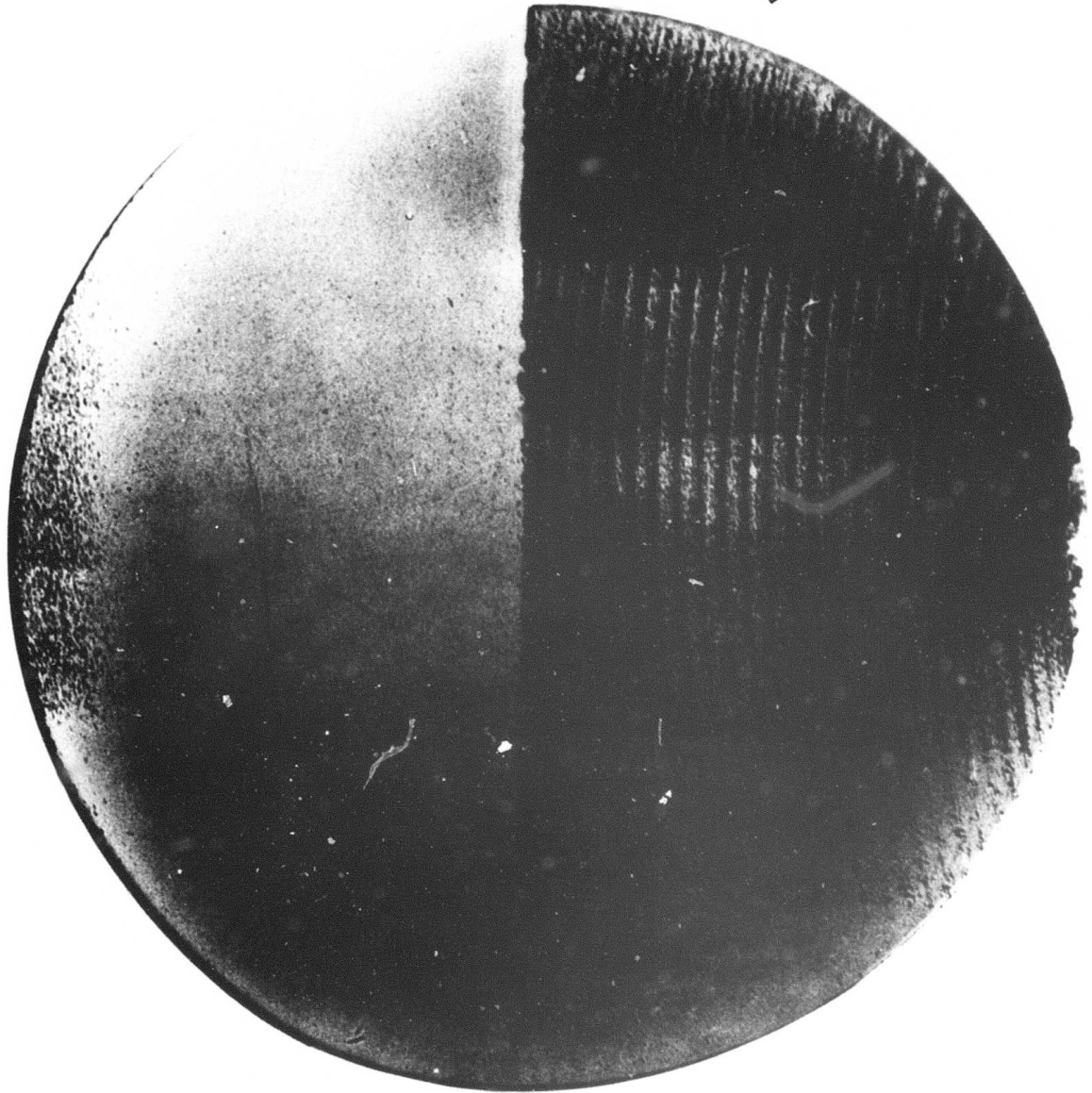


Fig. 8a. SOT topograph of damage in B wafer, middle cut.

DAMAGE MAP: MIDDLE B

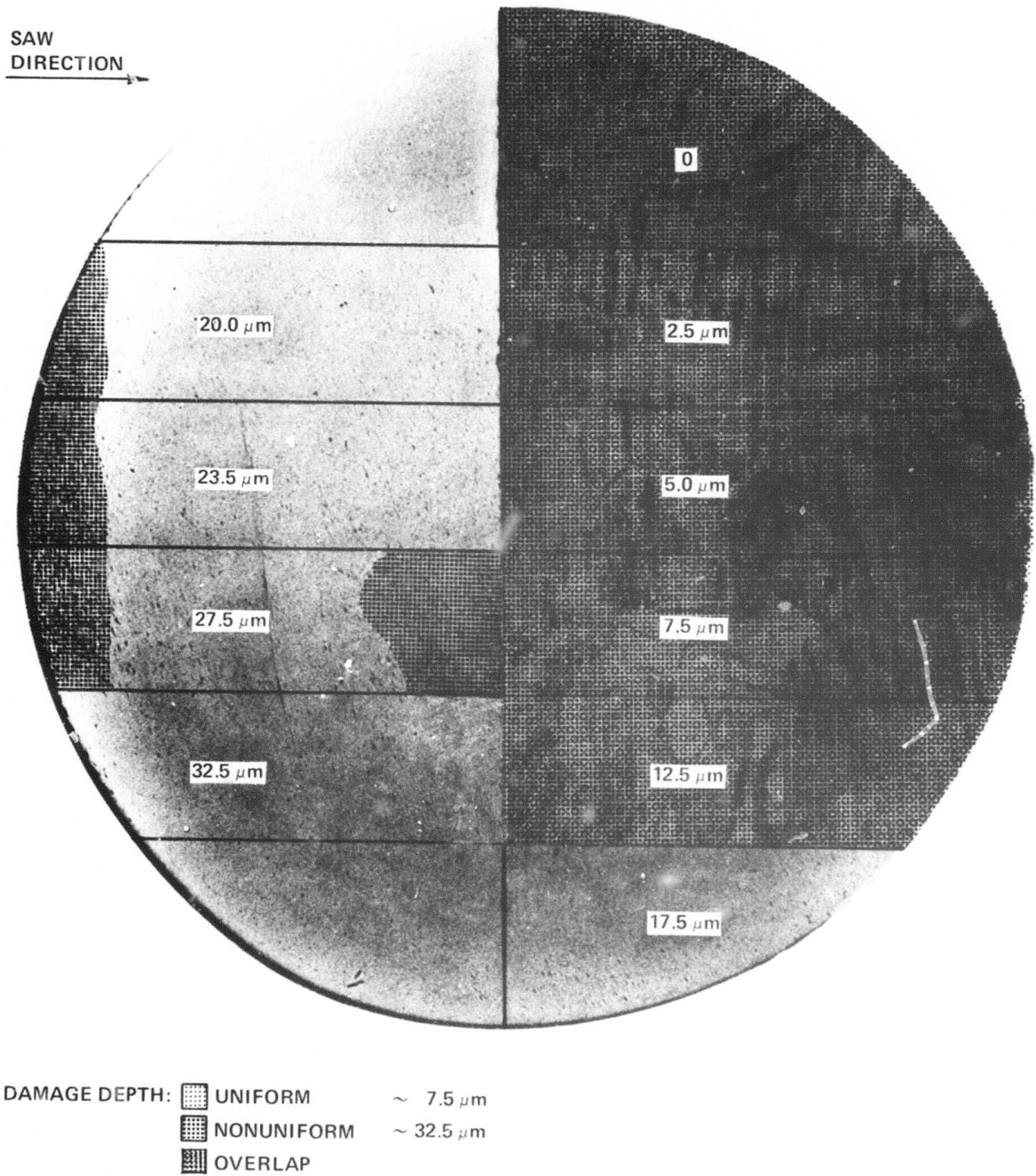


Fig. 8b. Damage map corresponding to Fig. 8a.

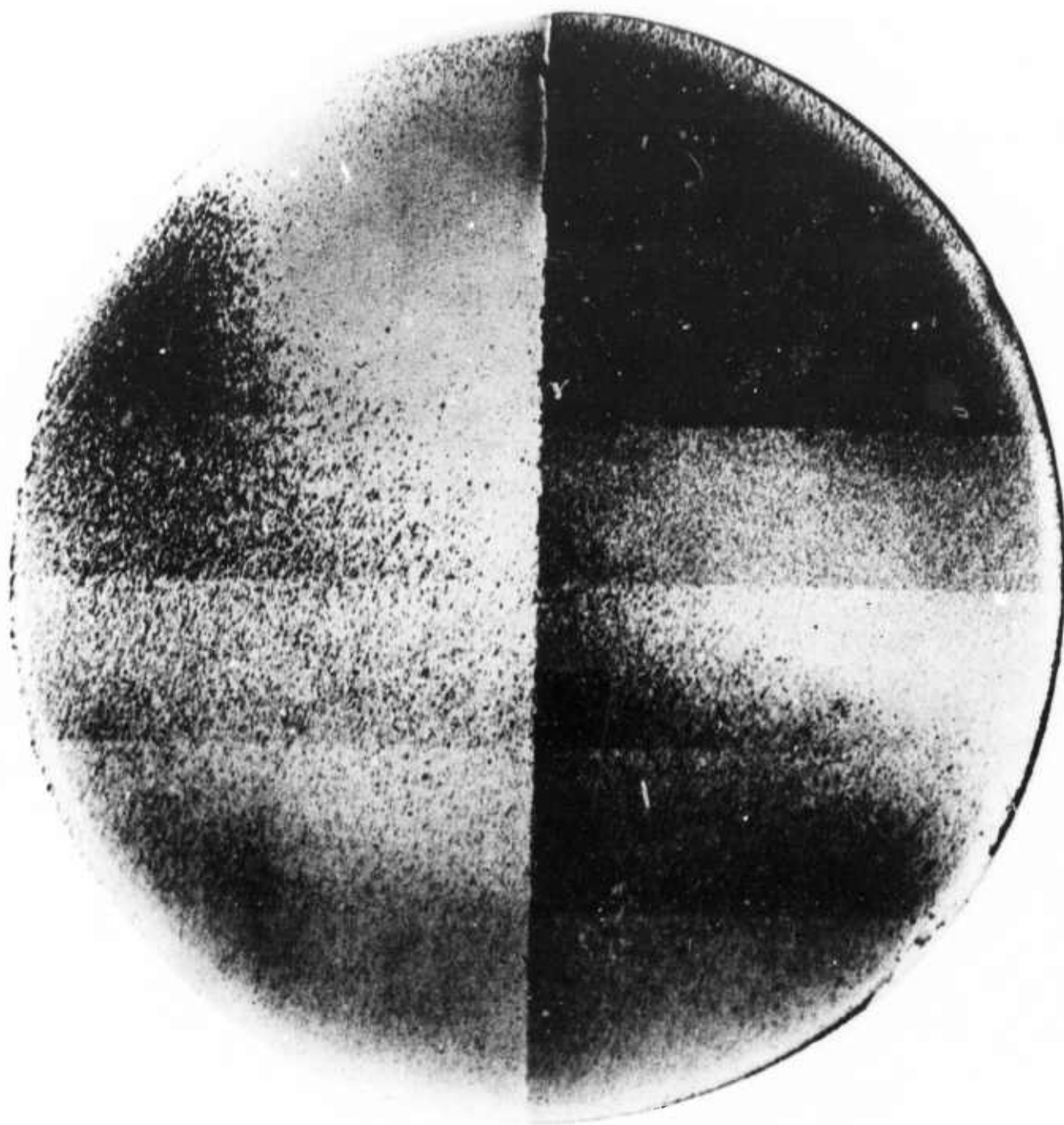
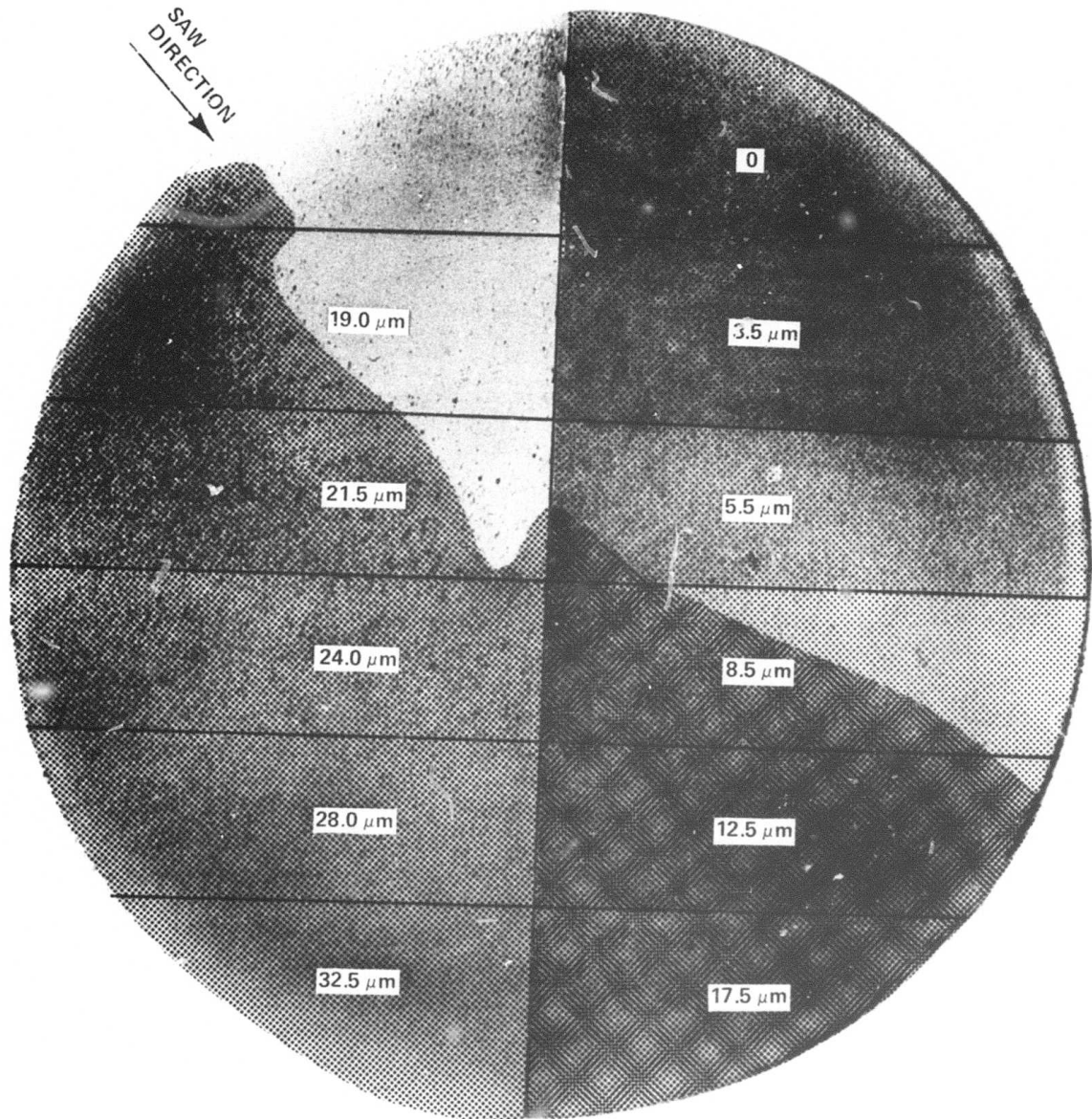


Fig. 9a. SOT topograph of A wafer, cut from end of crystal.

DAMAGE MAP: END A



DAMAGE DEPTH:  UNIFORM ~ 8.5 μm
 NONUNIFORM > 32.5 μm
 OVERLAP

Fig. 9b. Damage map corresponding to Fig. 9a.

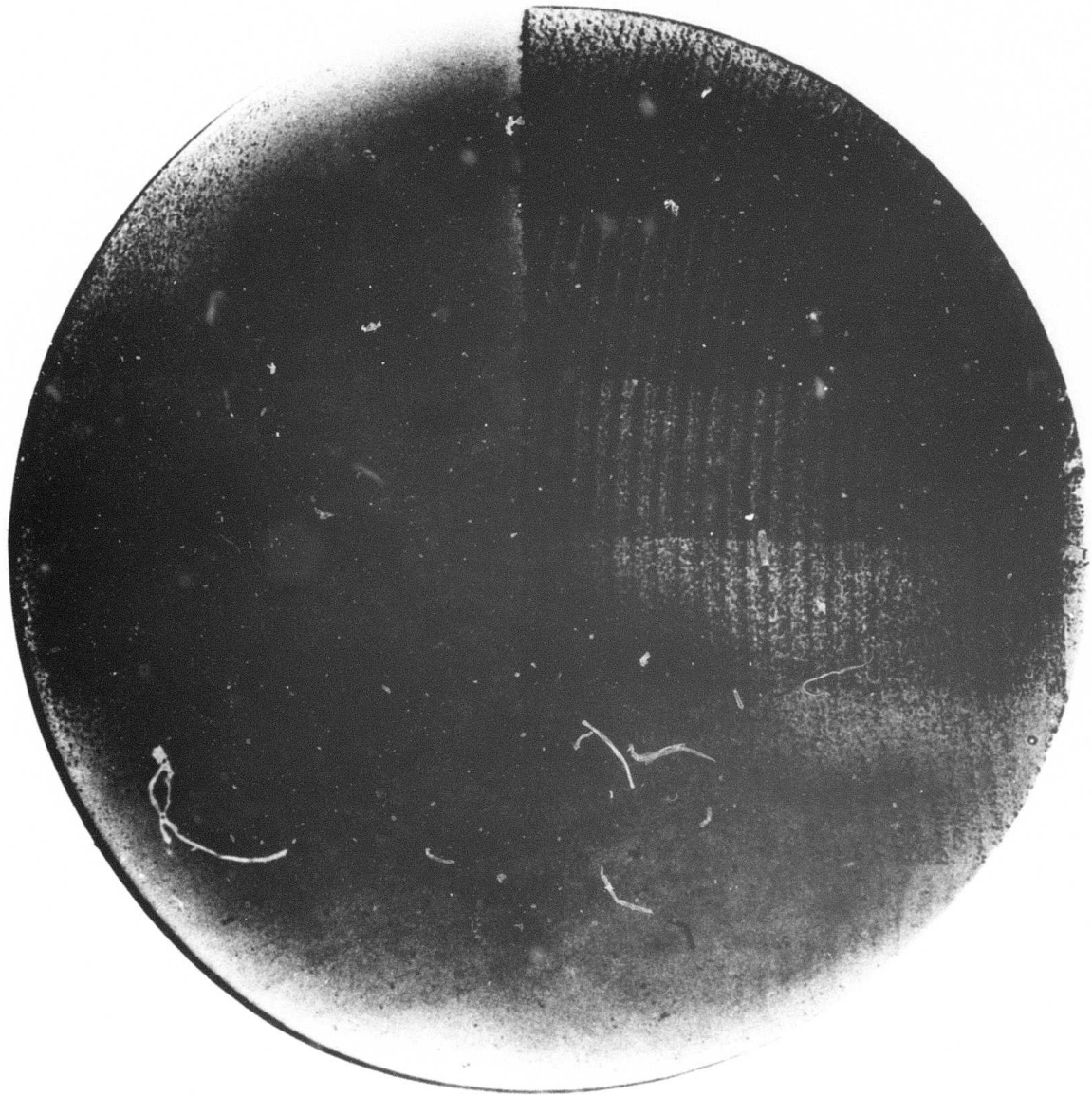
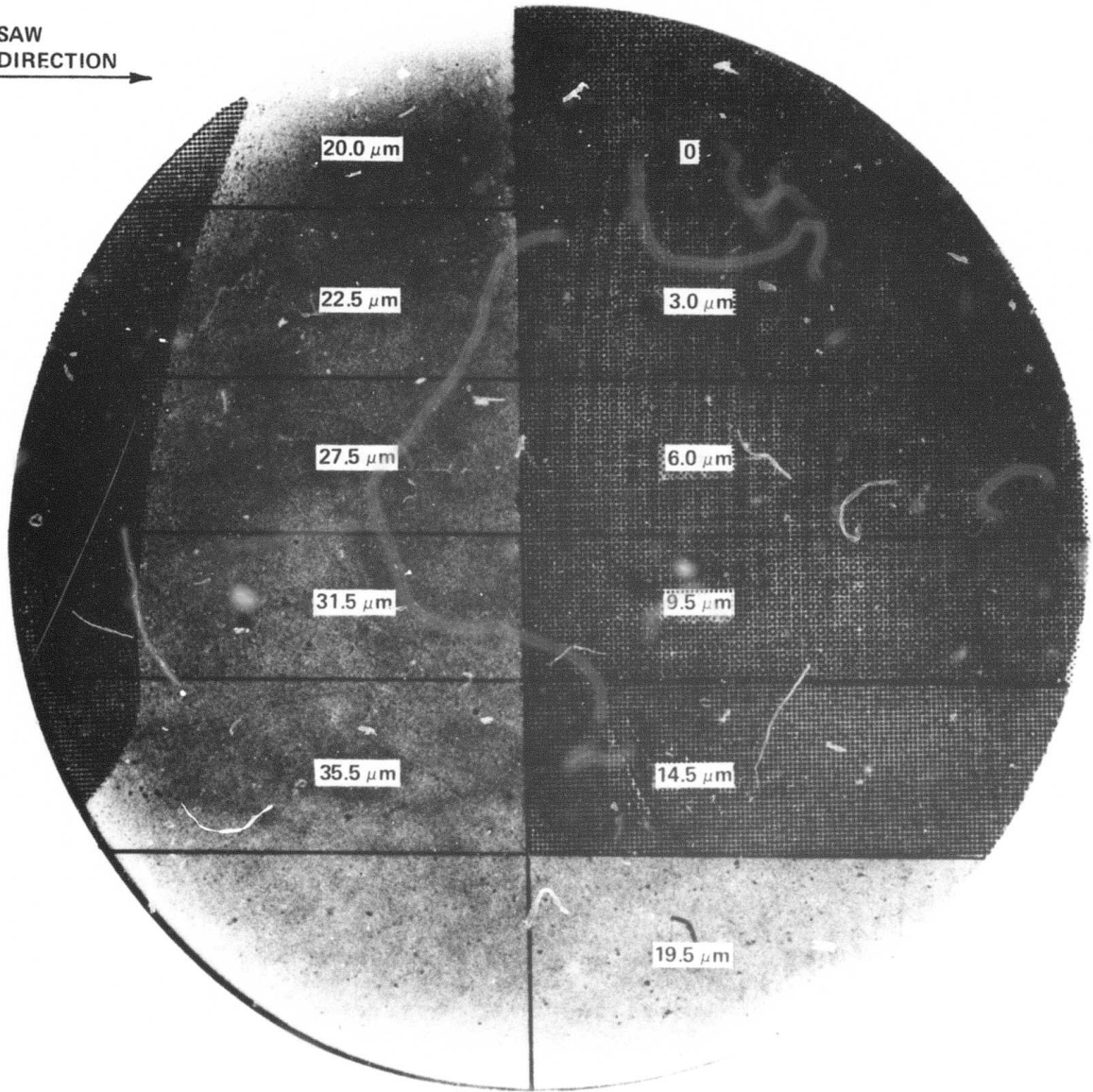


Fig. 10a. SOT topograph of B wafer, cut from end of crystal.

Reproduced from
best available copy.

DAMAGE MAP: END B

SAW
DIRECTION
→



DAMAGE DEPTH:  UNIFORM ~ 9.5 μm
 NONUNIFORM ~ 35.5 μm
 OVERLAP

Fig. 10b. Damage map corresponding to Fig. 10a.

4.3 Damage Profiles

An analysis of adjacent surfaces (separated by the saw blade during the same cut) permits a good evaluation of the slicing process in terms of saw damage. Such an evaluation is made through damage profiles. The damage profile of the wafer introduced by the sawing process is obtained through recording and evaluating SOT topographs with the help of damage maps of A and B slices taken at various locations along the crystal throughout the complete slicing procedure. Such damage profiles are shown in Fig. 11. Note that the major damage contribution comes from the nonuniform damage mode.

Significant in these profiles is also the variation of nonuniform saw damage depth with wafer position. In this experiment the nonuniform damage in the A surfaces appears higher than in the B surfaces.

Interesting are the damage depth curves obtained for the uniform damage. The uniform damage on A and B surfaces show an opposite trend. The damage in the A surfaces is larger in the beginning and is steadily decreasing while the damage in B surfaces is considerably smaller at the start than in the A surfaces but is steadily increasing. A and B surfaces are approaching the same damage depth of approximately $10\mu\text{m}$.

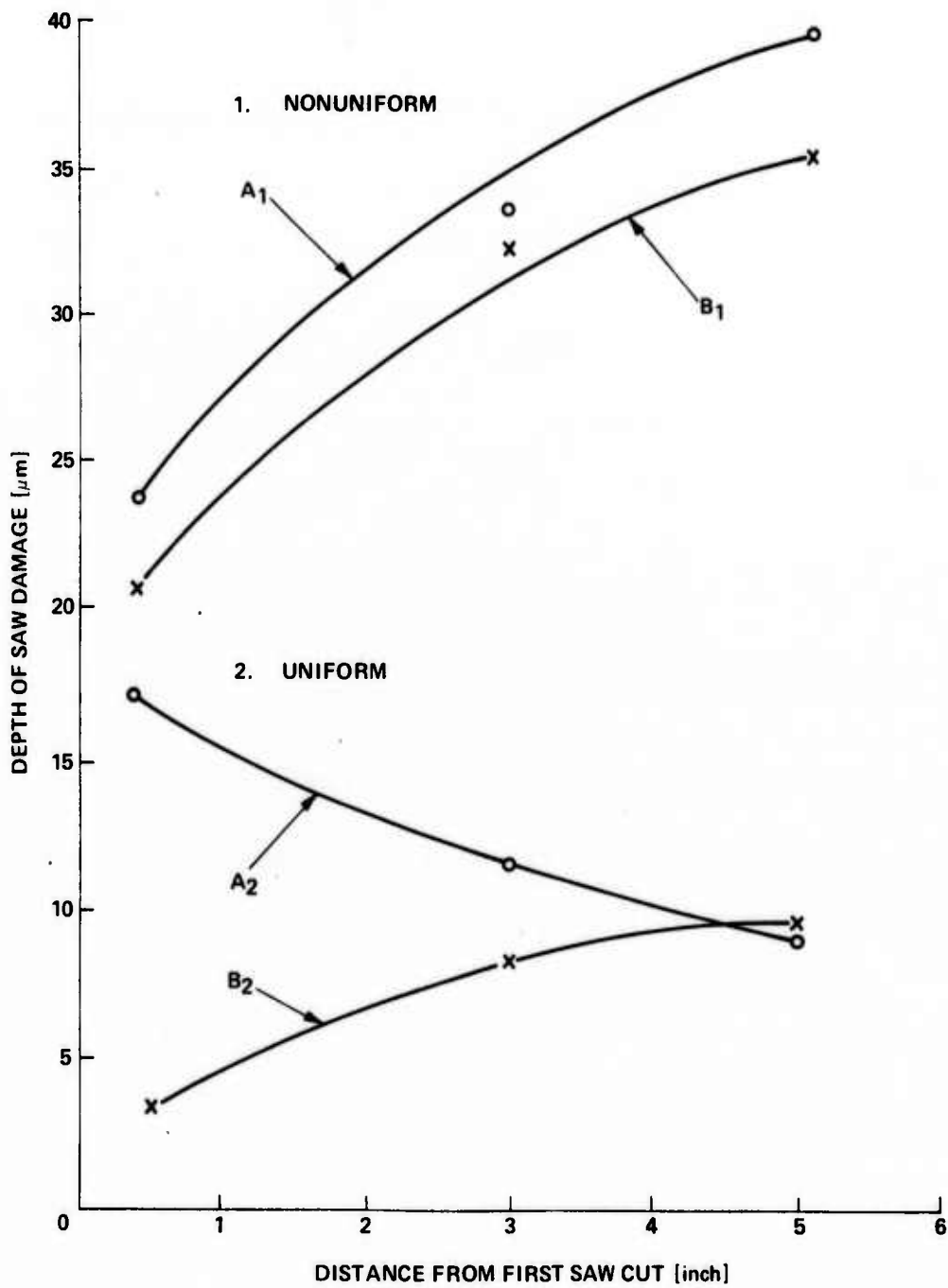


Fig. 11. Damage profiles showing damage distribution after slicing.

- 1. Inhomogeneous
- 2. Homogeneous

5. APPLICATION OF SAW DAMAGE MEASUREMENTS
TO H- AND V- SILICON WAFERS

Crystals used for this experiment were IBM grown of $\langle 100 \rangle$ orientation, 2 1/4 inch diameter and 15-20 ohm-cm resistivity. The crystals were sliced by two different vendors to obtain representative seed and tail wafers classified according to the slicing procedure and H- and V-wafers. The selected wafers were evaluated for "depth of damage" as discussed in section 4 using x-ray topography and damage maps. In support of the x-ray data uniform and nonuniform damage depth were also evaluated through the etch rate technique (uniform damage) and the taper section technique (nonuniform damage). All these data are compiled in Table III.

As shown in Table III the depth of uniform damage varies from $15\mu\text{m}$ - $20\mu\text{m}$ and is practically the same for the H- and V-wafers. No difference is observed for seed and tail wafers. Contrary, the nonuniform damage is found to vary considerably in V-sliced wafers from approximately $21\mu\text{m}$ to $63\mu\text{m}$, while in H-wafers this type of damage shows less spread and stays below $12\mu\text{m}$. This indicates, at least for this experiment, that H-wafers are sliced better controlled than V-wafers. Likewise, we find in this experiment the damage dependency on wafer position (seed to tail) again confirmed.

TABLE III

Depth of Saw Damage in H- and V- Wafers

ER - Etch-Rate Method; TS - Taper-Section Method;
SOT - X-Ray Method

Sample No.	Max. Depth [μ m] Uniform Mode		Max. Depth [μ m] Nonuniform Mode	
	ER	SOT	SOT	TS
V-wafer				
Seed 1	18.1	16.0	>45	
2	23.2	15.5	23.2	16.5
Tail 24	33.0	15.5	>63.0	46 to 51
25	21.3	19.8	21.3	
H-wafer				
Seed 1	14.8	16.4	>8.8	9.5
2	17.8	12.5	12.3*	
3	14.4	19.5	9.6	
Tail 24	16.6	20.4	16.8	
25	16.7	16.3	16.8	

* 2 saw marks extended deeper than 45 μ m. This was found unusual for H-wafers and therefore was not considered.

6. DISCUSSION

Damage profiles as shown in Fig. 11 are not necessarily representative of the state of the art of ID slicing of silicon. However, we have come to the conclusion that ID slicing of semiconductor crystals in general does not get the attention necessary to guarantee a minimum of damage in silicon wafers after slicing. Perfection of silicon wafers after slicing and polishing seems to be more or less accidental. Damage profiles after slicing are unknown and not asked for. Quality assurance of wafers is obtained after polishing and is based on optical inspection of specular surfaces. Such surfaces are classified as perfect but may contain millions of microsplits^{1,2} which are leftovers of saw damage introduced through ill-understood and badly controlled slicing.

High speed ID slicing techniques have seen very little or no improvement since their introduction to slice one inch thick silicon crystals. In the meantime silicon crystals have become three inches thick and the industry is already talking about the use of even thicker silicon crystals. So far the main objective of all manufacturing slicing techniques has always been to improve "throughput". Perfection of silicon after slicing has never been a concern because it did not seem to influence the final yield of good devices per wafer.

Future generations of semiconductor devices require the highest perfection possible in the silicon wafer after slicing and polishing. To achieve this goal, the slicing process must be recognized as an area of major concern. Major problems to be solved can be classified as follows:

1. Homogeneous and inhomogeneous distribution of damage in silicon wafers after ID slicing.
2. Variation of damage in wafers relative to the original wafer position in the crystal.

Problems listed under (1) are obviously technique and equipment related and, consequently, can be minimized or eliminated if properly understood. Damage profiles as presented in Fig. 11 appear very useful in this respect and are proposed for general application to achieve quality control of the ID slicing process. The inhomogeneous damage distribution in silicon wafers after ID slicing must be reduced to a minimum. This can be achieved as demonstrated by the damage distributions obtained in H-wafers as shown in Table III.

The inhomogeneous damage mode relates obviously to an ill-controlled slicing process. Flutter blade damage in the form of striations and peripheral damage at the point of initial blade contact as shown in Figs. 8 and 10 are a vivid example of what ID slicing should not be like. Changes of saw blade tension are responsible for the striation contrast displayed in the topographs of Figs. 8 and 10. The direction of curvature of the striations relative to the sawing direction suggests further that this type of damage occurs mainly during blade removal. This is in agreement with the polished appearance of the corresponding A surfaces (Figs. 7 and 9) which indicate abrasive contact with the convex side of the deflected blade. The strong edge damage of the B surface in Figs. 8 and 10 at the point of initial blade contact is also an indicator of either irregular blade removal and/or excessive feed rate.

The delicate interplay between the two above-mentioned main characteristics of the ID silicon crystal slicing process determines the amount of damage induced in the wafer. This is clearly demonstrated in wafers cut by different slicing techniques, such as H- and V-wafers. Blade deviations during cutting, variations in cutting speed, blade flutter, and blade tension are ID cutting parameters which deserve the best control possible in order to achieve minimum damage in wafers produced by high speed slicing of silicon. The "damage profile technique"

is proposed in this context as an elegant and useful technique to control, maintain, or obtain the best crystal slicing process and minimum damage in ID sliced silicon wafers.

7. SUMMARY AND CONCLUSIONS

A systematic approach for characterizing sawing procedures of crystals in semiconductor manufacturing is described. This practice relies on damage profiles obtained from the cut wafers. Such profiles can describe the entire slicing procedure of the crystal and are obtained through evaluation of SOT topographs of adjacent wafer surfaces.

This approach removes much of the difficulty encountered previously in achieving reproducible results of saw damage, as shown by the diversity of values listed for damage depth in Fig. 1. The depth of damage is evidently sensitive to numerous operational variables. The complex nature of saw damage follows from the damage profiles of the sliced crystal and the extensive variations in damage contrast displayed in the SOT topographs. Therefore, saw damage data must always be viewed in the context of the particular slicing technique.

Damage profiles of crystals cut by standard ID procedures reveal that the depth of uniform damage on either side of the crystal can vary up to 75%, and that the variation in damage depth depends

on the blade size, feed rate, spatial location of the wafer (seed to tail) and blade tension.

The nonuniform damage mode across the wafer is related to the direction of sawing and is much more pronounced in V-wafers relative to H-wafers. This damage mode is also recognized as being responsible for residual saw damage in wafers after chemical-mechanical polishing. For the purpose of process improvement, the damage profile method can be used advantageously to optimize sawing parameters — such as feed rate, cutting rpm, etc. and to reduce damage, specifically the nonuniform mode, to a minimum.

8. REFERENCES

1. G. H. Schwuttke, Technical Report No. 1, January 1973.
2. G. H. Schwuttke, Technical Report No. 2, July 1973.
3. J. W. Faust, *Electrochem. Tech.*, 2, 339, 1964.
4. E. N. Pugh and L. E. Samuels, *J. Electrochem. Soc.*, 108, 1043, (1964).
5. R. Stickler and J. W. Faust, *Electrochem Tech.* 4, 339, (1966).
6. R. Stickler and G. R. Booker, *Phil. Mag.* 8, 858, (1963).
7. T. M. Buck, *The Surface Chemistry of Metals and Semiconductors*, ed. H. C. Gatos, p. 107, John Wiley & Sons, Inc., New York 1960.
8. T. M. Buck, *J. Electrochem Soc.* 109, 1220, (1962).
9. G. A. Wolff, J. M. Wilbur and J. C. Clark, *J. Electrochem.* 61, 101, (1957).
10. J. W. Faust, in *Symposium on Cleaning of Electronic Device Components and Materials*, ASTM Spec. Tech. Pub. 246, p. 66, Phil., Pa., 1959.
11. G. H. Schwuttke, J. K. Howard and J. Regh, unpublished.
12. G. H. Schwuttke, *J. Appl. Phys.* 36, 2712, (1965).
13. E. J. Saccocio and W. McKeown, *J. Appl. Phys.* 37, 2702, (1967).
14. W. R. Runyan, *Silicon Semiconductor Technology* p 231, (McGraw Hill, N. Y. 1965).
15. T. M. Buck and F. S. McKim, *J. Electrochem. Soc.*, 105, 711 (1958).

FRACTURE STRENGTH OF DOPED SINGLE CRYSTAL SILICON

1. INTRODUCTION

Measurements reported in Technical Report No. 2, and Chapter 1 of this report indicate clearly that Czochralski grown silicon crystals show variations in residual saw damage after ID slicing such that more damage persists in wafers cut close to the tail end of the crystal relative to wafers cut close to the seed end. Such differences in damage sensitivity of Czochralski grown silicon can be understood if one postulates a variation in fracture strength of silicon crystal from seed to tail such that the seed part of the crystal is stronger than the tail section. To substantiate this contention, we have made measurements of the fracture strength of silicon. Such measurements are reported in the following.

2. EXPERIMENTAL APPROACH

To investigate the relative fracture strength of seed and tail ends cut from Czochralski grown crystals, we utilize the technique of Hertzian cone fracture combined with x-ray topographic evaluation of cone crack propagation. Hertzian fracture is preferred to more conventional types of fracture, such as cantilever fractures, because Hertzian fractures are considerably easier to

reproduce and almost identical fracture cones can be produced on a specimen surface under identical experimental conditions. The highly strain sensitive non-destructive technique of x-ray transmission topography is ideally suited for evaluation of subsurface crack propagation. Apart from typical geometrical features of the silicon surface under crack loading, the fracture process in the Hertzian test is essentially the same as in other tests so that Hertzian cone fracture can be taken as representative of brittle fracture processes in general.

3. TECHNIQUE DEVELOPMENT

Hertzian cone fracture patterns were produced by impacting polished silicon surfaces with free-falling, hardened and chrome-plated steel balls. An example illustrating Hertzian fracture cones in Si is shown in Figs. 1 and 2. Such measurements were made using a simple test setup where plastic tubes are positioned vertically above the silicon sample piece as shown in Fig. 3. The tubes served to hold the sample on the base plate and guide the steel balls. The balls were dropped into holes cut into the sides of the tubes (Fig. 4). The equally spaced holes allowed some experimental variation of the drop height. The balls were prevented from restriking the sample after rebound by insertion of a curved rod into a slot at the bottom of the tube. (Fig. 5) This rod also served to subsequently raise the balls to



Fig. 1. Partially exposed Hertzian fracture cone in monocrystalline silicon. Ball diameter 22.2mm drop height 63.5cm, slice thickness 10mm. Top view of sample (10.5X).

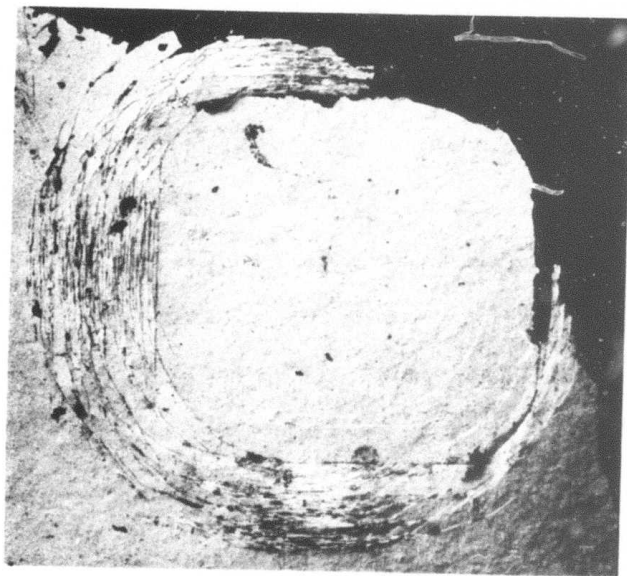


Fig. 2. Close-up of surface ring cracks in sample shown in Fig. 1 (46X).

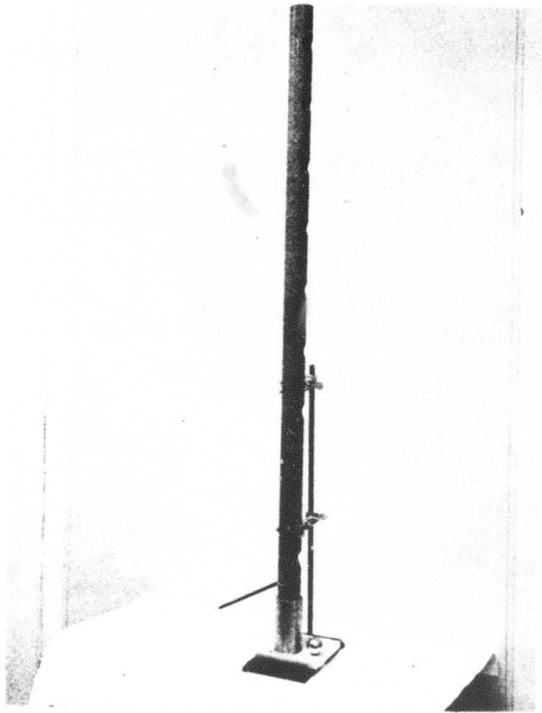


Fig. 3. Drop tube and steel ball for Hertzian fracture cone production in silicon (test slug is shown in place).

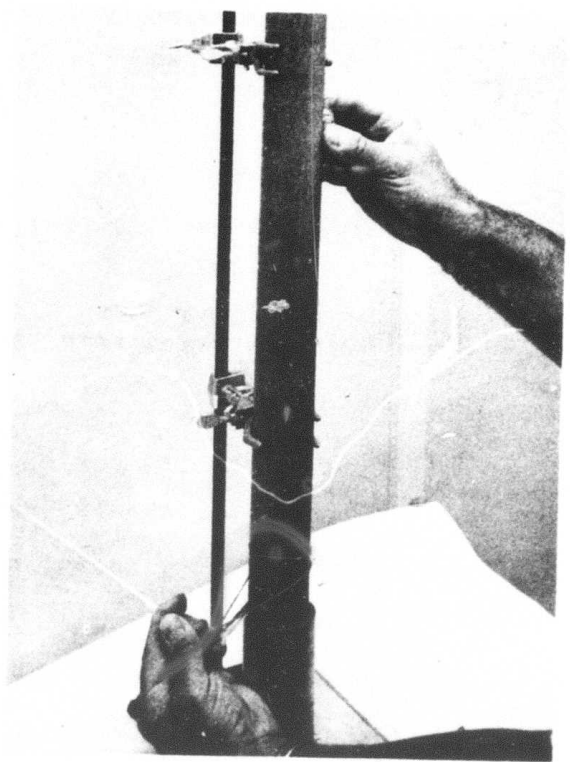


Fig. 4. Fracture cone production in progress.

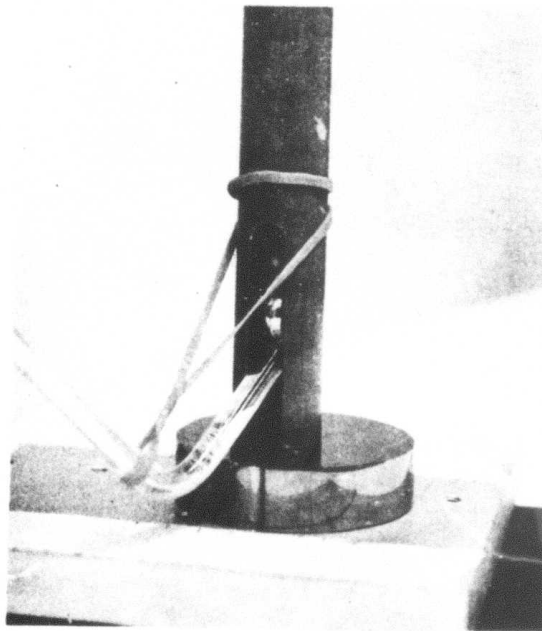


Fig. 5. Means for preventing a second impact after rebound of steel ball.

the removal hole where they were taken from the tube by a magnet. (Fig.6) This facilitated repositioning of the sample slug for the next drop. Various size balls with the appropriate tubes were used (Fig.7) to obtain a range of crack sizes.

The silicon material used was cut from P type, 2 Ω -cm <100> oriented single crystals ground to a diameter of 2 1/4 inches. Each sample slug had a minimum thickness (height) of 3mm so that it would not shatter upon impact. The test depends on the amount of energy impacted to the sample slug according to drop height and weight of ball. The drop height must be sufficient so as to produce enough rebound for subsequent restraint of the ball. Excessive energy may cause cleavage at the point of impact or complete shattering of the slug.

For sample preparation, both sides of the sample slugs were lapped with 600 grit silicon carbide powder to give uniform surfaces parallel to within one millimeter. The surfaces were then chemically polished for ten minutes in an agitated mixture. The polishing mixture consisted of 3 parts nitric acid, 2 parts acetic acid, and 1 part hydrofluoric acid (49%).

A number of experimental runs were made and the diagonal distances to the outside of the ring crack patterns were recorded. These measurements varied from 0.59 mm, obtained with a 6.4 mm

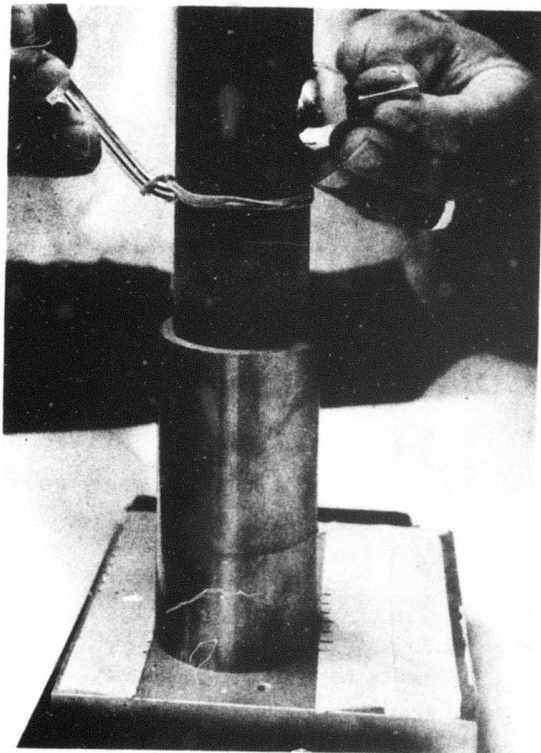


Fig. 6. Method of removing ball from drop tube prior to relocating sample for next impact.

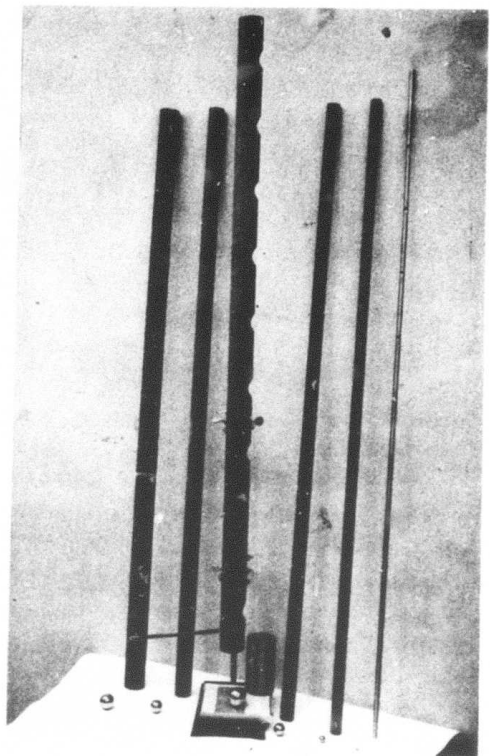


Fig. 7. Various size drop tubes and steel balls for fracture cone production.

diameter ball dropped from a height of 50.8 mm, to a diagonal of 3.36 mm with a 34.9 mm ball dropped 63.5 cm. The slug thicknesses for these were 3 mm and 150 mm, respectively. Ring fracture patterns considerably larger than those reported in the literature⁴ were thus produced in silicon.

In silicon, as in diamond, the ring cracks follow crystallographic directions at the surface. They penetrate the material along cleavage planes at crystallographically determined angles with the surface, thus forming the fracture cones (Figs. 1 and 2).

In the present work, a measure of the size of the fracture cone base within the material is taken as an indication of fracture strength. Projections of the fracture cone bases were obtained by x-ray transmission topography. Sample preparation for this was as follows. The test slugs after impact were cut down to a 2 mm thick slice to facilitate x-ray transmission. The surface containing the fracture cones was protected with a white wax and the back side lapped and chemically polished as described previously. The removal of saw damage from the back side is necessary to prevent x-ray contrast interference with the fracture cone pattern in the x-ray topograph. The wax is removed prior to mounting the slice in the sample holder. The (220) and the (111) reflections are used for x-ray topograph

recording. The (111) reflection was used exclusively for the study of relative fracture strength of seed and tail sections. Topographs were recorded on Ilford nuclear plates type G5, 50 μm thick emulsion, with molybdenum K_{α} radiation.

An example of a Hertzian fracture cone in a 0.375 mm thick silicon wafer is shown in Figure 8a and its topographic image is seen in Fig. 8b.

4. MEASUREMENTS OF FRACTURE STRENGTH ON SEED AND TAIL SECTIONS OF SILICON CRYSTALS

Slugs used for the seed and tail end measurement were cut from P-type, $\langle 100 \rangle$ oriented crystals. Table I lists particulars of the crystals. The sample slugs were lapped and polished

TABLE I

Crystal No.	Length [cm]	Resistivity [Ω -cm]		Diameter in cm	
		Seed	Tail	Seed	Tail
1	30.5	5.00	4.00	6.3	6.3
2	33.0	2.00	1.40	6.4	6.4
3	38.1	7.00	4.30	6.1	6.2
4	21.6	1.90	1.74	6.1	6.2

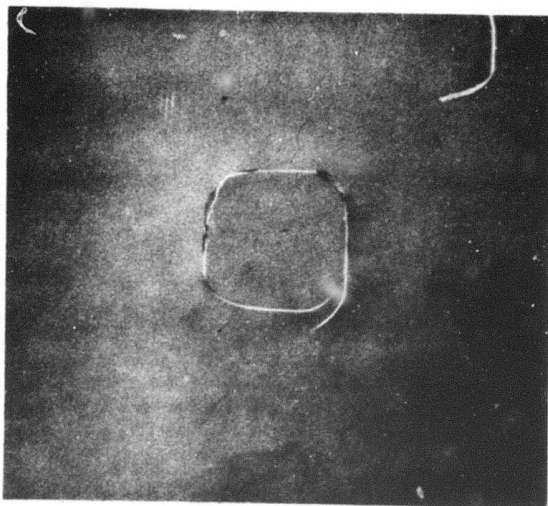


Fig. 8a. Photo micrograph of Hertzian fracture ring in 0.375mm thick silicon wafer, ball dropped 21.6cm (46X).

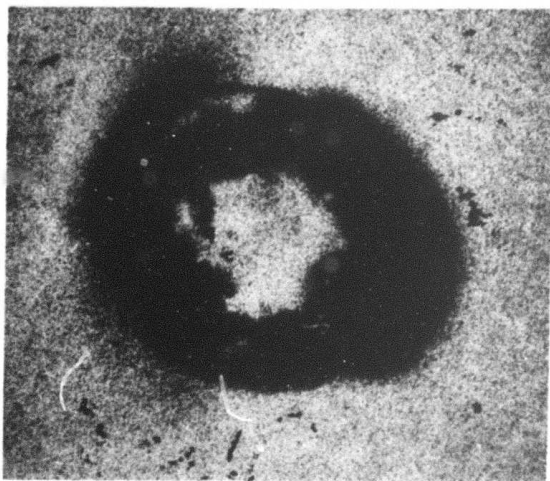


Fig. 8b. X-ray topograph of Hertzian fracture cone shown in Fig. 8a. Note larger dimensions (46X).

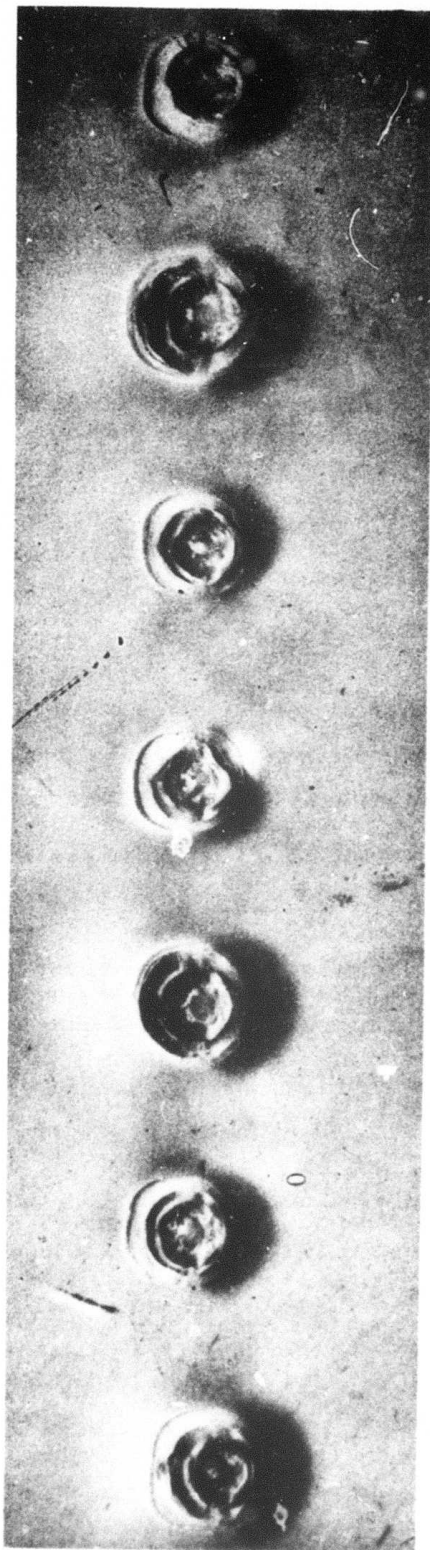
as described in Section 3. The experimental parameters chosen were slug height: 22 mm; ball diameter: 12.7 mm; and drop height: 56 cm.

Seven fracture cones were produced on each seed end slug and on each tail end slug. The cones were spaced 7 mm apart from the center of the slug along a diameter in a $\langle 110 \rangle$ direction.

X-ray topographs were taken as described above to outline the projections of the subsurface cone bases.

A typical example of such a test series is shown in Fig. 9.

The sizes of surface ring crack patterns and cone base projections, used as indicators of relative fracture strength, were obtained from enlarged micrographs of the samples and enlarged x-ray topographic plates, respectively. The measurements on both were made according to a scheme shown in Fig. 10. The average pattern diameter (D) for the seven fracture cone tops and bases on each test slug was calculated from this data with the expression:
$$D = \sum_{n=1}^7 \frac{(a_n + b_n + c_n + d_n)}{28}$$



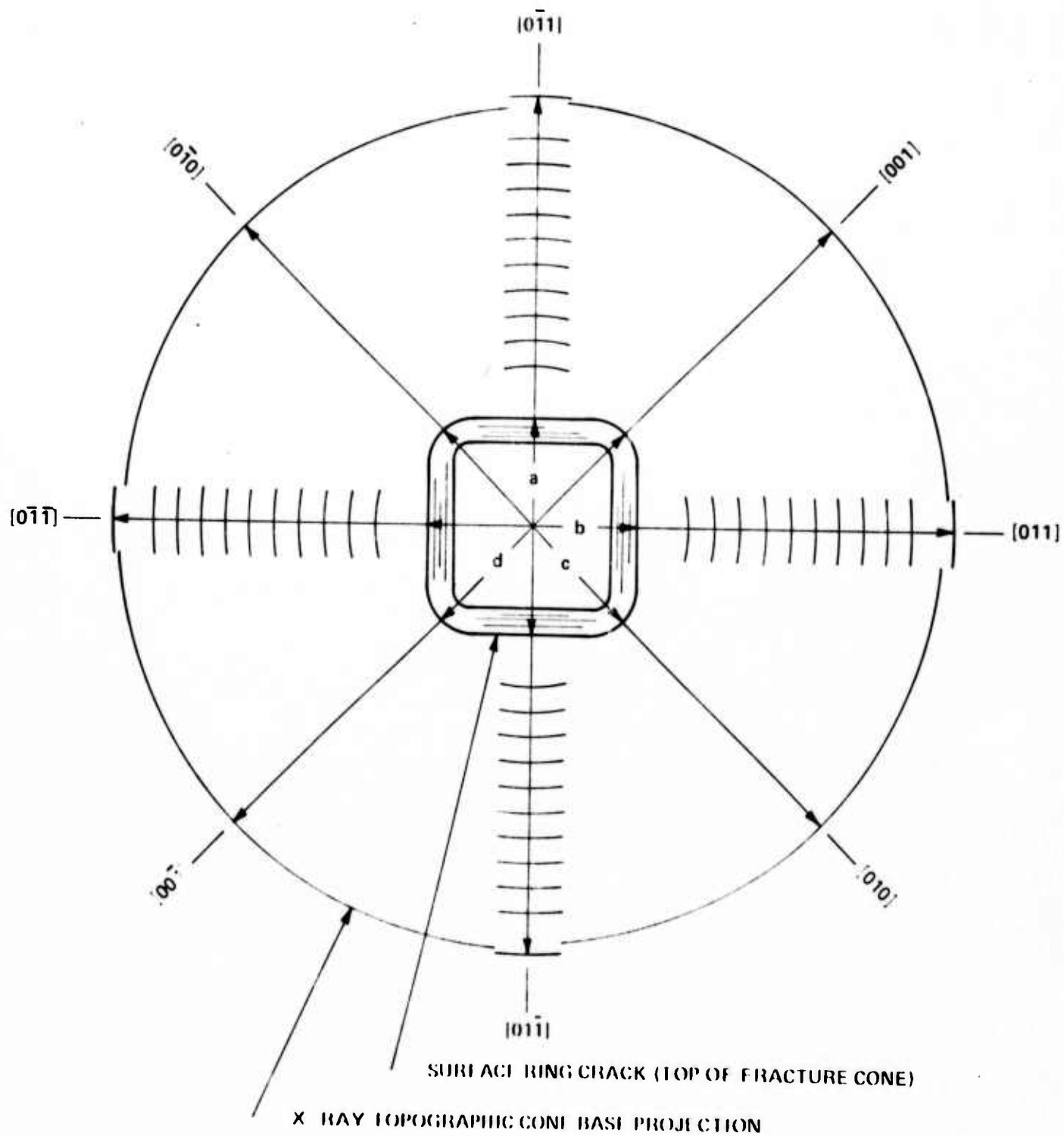


Fig. 10. Measurement scheme for ring crack patterns and fracture cone base projections.

TABLE II

Crystal No.	D (optical) in mm		D (x-ray) in mm	
	Seed	Tail	Seed	Tail
1	1.22	1.19	3.85	3.88
2	1.16	1.20	3.64	3.86
3	1.16	1.20	3.82	3.91
4	1.18	1.22	3.25	3.75
Average	1.18	1.20	3.64	3.85

Table II gives the average surface crack ring diameters and the average subsurface fracture cone base projection diameters for the seed and tail parts of the four crystals.

Table II shows that the average subsurface fracture cone base projection diameters for seed parts are consistently less than for tail sections. This indicates that the fracture cones progressed deeper into the tail slugs thus indicating less fracture strength.

The results also show that the fracture cone base projections obtained by x-ray topography are considerably more reliable for evaluating cone fracture than the surface ring cracks.

It can be seen from Table II that the 4-crystal average of surface ring crack diameter for tail sections exceeds that of seed sections by only 1.7%. However, the average of fracture cone projection diameters on the tail parts exceeds that of the seed slugs by 5.8%. This is also illustrated in Figs. 11, which show two standard fracture cones produced during the experiment. The inside diameters of the crack rings are approximately equal (Figs. 11a, b), while the x-ray topographs are decidedly different in size (Figs. 11c, d). The deeper fracture cone (Fig. 11a) has a multiplicity of cracks in the surface and the outside surface diameter is only about 20% larger than that of the cone shown in Fig. 11b. The corresponding topographs of these two cones are shown in Figs. 11c, d. It can be seen that in the x-ray topograph the cone corresponding to Fig. 11a is about 74% larger than that of the cone shown in Fig. 11d. This illustrates again the greater sensitivity of x-ray topography measurements for fracture evaluation. Furthermore, in the optical inspection of impacted surfaces, not all cracks may be equally visible at a given Nomarski contrast setting. This is due to the fact that the tops of Hertzian fracture cones are typically raised irregularly above the sample surface. Therefore, even if the ring crack patterns are viewed and photographed at various contrast settings, measurement errors can easily occur. This may be the reason for the reversed optical measurements data listed for Crystal #1. There is no doubt that the x-ray topograph gives a much more definite pattern for measurements than the crack ring micrograph.

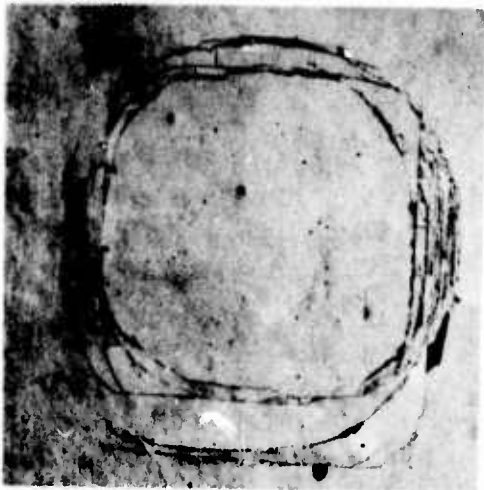


Fig. 11a. Optical micrograph of standard fracture cone produced on tail section (46X).



Fig. 11c. X-ray topograph of fracture cone corresponding to Fig. 11a (approx. 10X).

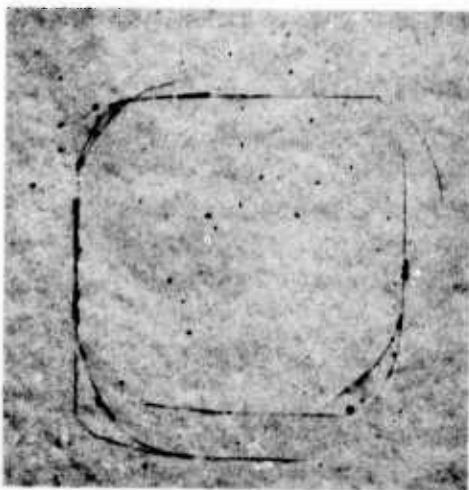


Fig. 11b. Optical micrograph of standard fracture cone produced on seed section (46X).



Fig. 11d. X-ray topograph of fracture cone corresponding to Fig. 11b (approx. 10X).

5. CONCLUSIONS

Hertzian fracture cones are used as a measurement of relative fracture strength in doped silicon single crystals.

A convenient and sensitive method for obtaining a measure of cone depth is the production of a cone base projection by means of x-ray topography.

Fracture strength of seed parts of Czochralski grown silicon monocrystals exceeds that of tail ends.

6. REFERENCES

1. S. Tolansky and A. Halperin, Proc. Phys. Soc. B67, 473 (1954).
2. S. Tolansky and V. R. Howes, Proc. Phys. Soc. B67, 467, (1954).
3. V. R. Howes and S. Tolansky, Proc. Roy. Soc. A230, 287, (1955).
4. I. D. Kirvalidze, Soobshcheniya Akademii Nauk Gruzinskoi SSR, Vol. 43, pp. 57-62, (1966), Translator - Carl Demrick, Assoc.
5. F. W. Preston, Trans. Optical Soc. London Vol. 23, 141, Part I, Sec. I, (1921-22).